Applied Geochemistry 169 (2024) 106046

Contents lists available at ScienceDirect

Applied Geochemistry

journal homepage: www.elsevier.com/locate/apgeochem

Hydrogeochemical and isotopic characterization of the main karst aquifers of the middle Valseriana (Northern Italy): Nossana and Ponte del Costone springs

Andrea Citrini [a], Adriano Mayer [b], Corrado A.S. Camera [a,*], Anita Erőss [c], Jürgen Sültenfuß [d], Guido Pezzera [e], Giovanni Pietro Beretta [a]

[a] Dipartimento di Scienze della Terra "Ardito Desio", Università degli Studi di Milano, Milan Italy
[b] Département d'Hydro-Géologie, Avignon - Université, Avignon, France
[c] József and Erzsébet Tóth Endowed Hydrogeology Chair and Foundation, Department of Geology, Institute of Geography and Earth Sciences, ELTE Eötvös Loránd University, Budapest, Hungary
[d] Helium Isotope Laboratory, Institute for Environmental Physics, Universität Bremen, Bremen, Germany
[e] Freelancer, Seriate, Italy

ARTICLE INFO

Editorial handling by: Dr C S Eckley

Keywords:
Valseriana valley
Hydrogeological characterization
Karst systems
Nossana and Ponte del Costone springs
Helium isotopes
Groundwater residence time

ABSTRACT

Karst springs are one of the most exploited drinking water resources in the world. Isotopic and chemical analyses on these waters reveal essential insights into their hydrodynamics. Valseriana (Northern Italy) is a valley within the Italian Pre-Alps, characterized by high water availability. The main reasons are a bedrock consisting of very permeable carbonate formations and a mean annual precipitation above 1800 mm/y. In this context, the Valseriana spring catchments have become strategically important for the water exploitation and the domestic supply of Bergamo and the neighboring municipalities. This study general aim is to expand the knowledge on the two main karst systems (Nossana and Ponte del Costone), which together include twenty-three major and minor springs, by defining a state-of-the-art that will be useful in future decades to preserve this crucial resource. Specific objectives include i) verifying the applicability of the $^{3}H/^{3}He$ dating method in karst environments, ii) defining groups of springs according to their chemical and isotopic characteristics for possible safeguard actions, and iii) establishing a conceptual model of the internal dynamics of the two spring systems. A chemical and isotopic sampling campaign was specifically conducted between May 2018 and July 2019. A total of 34 water points were sampled, including natural springs, rivers, wells, karst caves, and nearby mines. Water sampling for $^{3}H/^{3}He$ isotopic analyses was proved possible through careful selection of the sampling points and the insertion of the pump tubing in the spring fractures. A first classification of springs into uniform hydrochemical groups was obtained by applying the hierarchical cluster analysis technique on major ions contents. These outputs were combined with information from the $^{3}H/^{3}He$ dating analyses and resulted in three different classes of springs. The three classes showed a clustering for elevations: at high, medium, and valley bottom elevations, respectively. Finally, the elaborations simplified the two karst systems by a hierarchical flow system model, dynamically controlled by different karst network development and infiltration water.

1. Introduction

Karst aquifers are one of the most exploited drinking water resources in the world (Ford and Williams, 2007) reaching about 678 million people, corresponding to 9.2% of the world's population (Stevanović, 2019). In detail, carbonate aquifers cover 15.2% of the global ice-free continental land surface (Goldscheider et al., 2020). The ease and affordability of their capture make them a strategic asset for companies managing water distribution for drinking and domestic use (Kollarits et al., 2006; Stevanović, 2019). Water quality and all measures to preserve and monitor it are critical to ensure a reliable integrated water service. Understanding the interaction between surface water and

* Corresponding author.
E-mail addresses: andrea.citrini@unimi.it (A. Citrini), adriano.mayer@univ-avignon.fr (A. Mayer), corrado.camera@unimi.it (C.A.S. Camera), eross.anita@ttk.elte.hu (A. Erőss), suelten@uni-bremen.de (J. Sültenfuß), pezzerag@virgilio.it (G. Pezzera), giovanni.beretta@unimi.it (G.P. Beretta).

https://doi.org/10.1016/j.apgeochem.2024.106046
Received 1 September 2023; Received in revised form 30 April 2024; Accepted 16 May 2024
Available online 23 May 2024

groundwater is crucial for a sustainable use of the resource, as well as studying its evolution in a global water framework threatened by the effects of climate change and land use (Citrini et al., 2020; Hartmann et al., 2014).

A conceptual model derived from a comprehensive hydrogeological study is essential when studying water availability and planning its management (Liu et al., 2007). A fundamental part of such a comprehensive study consists of the monitoring of water quality and the analysis of its chemical and physical parameters (Asante et al., 2018; Hamad et al., 2018; Yuan et al., 2017). Regarding springs, the association of physicochemical parameters with inflow and outflow regimes provides information on recharge processes, storage capacity, and the behavior of the aquifer as a whole (Vesper and White, 2004; Ryan and Meiman, 1996). The combination of major ions content and stable isotope ratios (e.g., hydrogen, oxygen, carbon, nitrogen, and sulfur) in water samples allows a general understanding of the internal dynamics of complex catchments (Erőss et al., 2012; Long et al., 2012; Marfia et al., 2004; Pu et al., 2014). Furthermore, the development of techniques that exploit the characteristics of radionuclides and environmental tracers (e.g., SF_6, CFC, $^3H/^3He$, ^{85}Kr and ^{39}Ar) allows to determine additional information concerning the residence time of groundwater in an aquifer system (Andrews, 1985; Cook and Böhlke, 2000; Gardner and Heilweil, 2014; Ozyurt, 2008; Pearson, 1991).

This study focuses on the results of the hydrochemical monitoring carried out between 2018 and 2019 on the waters of the main springs of the middle Valseriana (northern Italy, Province of Bergamo): Nossana and Ponte del Costone. The issue of ensuring safe water for the city of Bergamo has been profoundly concerning since the early decades of the 1900s, when water demand, due to urban development and population growth, reached the point that cisterns and small springs could no longer meet it (Mainoli, 1934). Hence, the distribution network was extended by acquiring aqueducts from adjacent municipalities so to connect the city with the springs of the middle Valseriana valley: in 1959, the Ponte del Costone springs in Casnigo, and in 1975, the Nossana spring in Ponte Nossa (Capellini, 1990). In recent years, events such as the atrazine crisis of the 1980s in the Po Plain demonstrated the strategic, ever-increasing importance of these springs (Beretta et al., 1989; Fioretti et al., 1998; Vighi et al., 1991). Furthermore, the presence of a large mining park in the North-West of the study area (Assereto et al., 1977; Mehta et al., 2020) and the industries located in the valley bottom represent a potential threat for the protection of these two main spring systems, which feed about 500,000 people in the Bergamo area.

Moreover, given the scientific evidence of changes in precipitation and temperature regimes (Citrini et al., 2020; Hegerl et al., 2015; Hosseinzadehtalaei et al., 2020; IPCC, 2014), it is crucial to define the current hydrogeological and hydrogeochemical status of these systems, to obtain a solid reference for future investigations with methods that can be applied repeatedly for monitoring purposes. Starting from the solid background of previous work conducted in the study area (Citrini et al., 2020, 2021; Gattinoni and Francani, 2010), this landmark survey by combining standard hydrochemical analyses, interpreted through statistical methods, and water dating through $^3H/^3He$ investigations will provide valuable insights regarding water age and quality. $^3H/^3He$ dating technique is normally used to define the apparent age of groundwater less than 40 years old (Delbart et al., 2014). In karst aquifers, because of the possible diffusion of light noble gases, (e.g., ^3He) from water to the internal air component of the vadose zone, this approach is considered challenging. In detail, the $^3He/^4He$ ratios are uncertain due to the uncertainties related to the radiogenic helium sources (Gil-Márquez et al., 2020). Specific objectives were.

- To assess the applicability of the $^3H/^3He$ dating method in a karst environment, testing it in this study area.
- To define groups of springs according to their chemical characteristics and estimated residence time to determine a kind of action priority and safeguard a specific cluster should water availability or water quality-related problems arise.
- To establish a conceptual model of the internal dynamics of the two main spring systems in the area.

2. Study area

The study area is in Valseriana, one of the most important valleys of Bergamo Province (Northern Italy). Valseriana is located in the Lombardy Pre-Alps and its valley bottom is characterized by the Serio River (Fig. 1). Specifically, this study will focus on the hydrogeological catchments of Nossana and Ponte del Costone springs. These catchments cover a wide elevation range (from about 420 m a.s.l. at the valley floor to 2512 m a.s.l. at the peak of Arera Mount) over a total area of about 90 km^2. They are separated from each other by the Val del Riso, an accessory valley historically of mining importance. In detail, in the area, an Alpine-type Zinc–Lead–Silver stratabound ore deposit was exploited until 1982 (Mondillo et al., 2020; Omenetto and Vailati, 1977).

The whole environment is dominated by the calcareous-dolomitic carbonate series, but although these two catchments are contiguous, they show relevant differences from a geological point of view. Nossana is one of the most important springs in Northern Italy regarding discharge rates (Citrini et al., 2020). Its catchment presents Ladinian - Carnian age formations, and the principal aquifer is set in the Calcare di Esino formation (Jadoul et al., 1985, 2012), a carbonate platform limestone series. The water system of Ponte del Costone is formed by 13 springs distributed over about 1 km along the Serio River. The catchment is composed of dolomite formations (the Dolomia Principale Formation, Norian age) as reservoir rocks (GeoTer, 2000; Ecogeo S.r.l., 2007; Jadoul et al., 2012; Spada and Bertuletti, 1988). The 13 springs are geographically distinguished into three areas (from south to north): the Galleria del Costone (from Costone 1 spring to Costone 7 spring), Merlo (Merlo Sud and Merlo Nord), and Bosco (Rocce, Foppone, Sottoplatea, and Bosco). These spring groups are separatedd by the Nossana spring basin because of a tectonic lineament of regional importance, the Clusone Fault, on which the course of the Riso River runs (Stevenazzi et al., 2023) (Fig. 1).

The two carbonate formations that primarily characterize the Nossana and Ponte del Costone catchments react differently to karst dissolution (Federazione Speleologica Lombarda, 2011; S.-J. Wang et al., 2004). The aquifer of the Nossana spring is a dominant drainage water system (double permeability) (Vigna and Banzato, 2015) marked by discrete large karst conduits within the Calcare di Esino. For the Costone system, the karst phenomena on Dolomia Principale act mainly on the pre-existing fractures, expanding them slowly, creating a dispersive percolation system (within pervasive lower-aperture fractures). The result of this contrasting situation can be observed in the discharge hydrographs of the main springs of the two systems, which are not comparable in magnitude and in their response to rainfall episodes. The Nossana spring has an average flow rate of 3.77 m^3/s, with peaks following intense rainfall events (response in one to 2 h) that reach 18 m^3/s; the sum of the discharges of the Ponte del Costone springs system is more constant and cannot be clearly correlated with rainfall events, averaging 0.25 m^3/s, with peaks up to 0.45 m^3/s (Citrini et al., 2021). In addition to these main springs (captured to provide water service to the city of Bergamo), many secondary springs, locally exploited by municipalities or for private uses, have an average discharge rate between 0.02 and 0.05 m^3/s (e.g., referring to Fig. 1, P-Berlina and U-Caalù springs located at high elevation in the Costone basin).

From the climatic point of view, the middle Valseriana is an area historically characterized by abundant precipitation with an annual average rainfall of about 1800 mm (Ceriani and Carelli, 2000). This climatic condition, in combination with an efficient carbonate environment subject to the karst phenomenon, leads to important water availability and a strategic area for water supply.

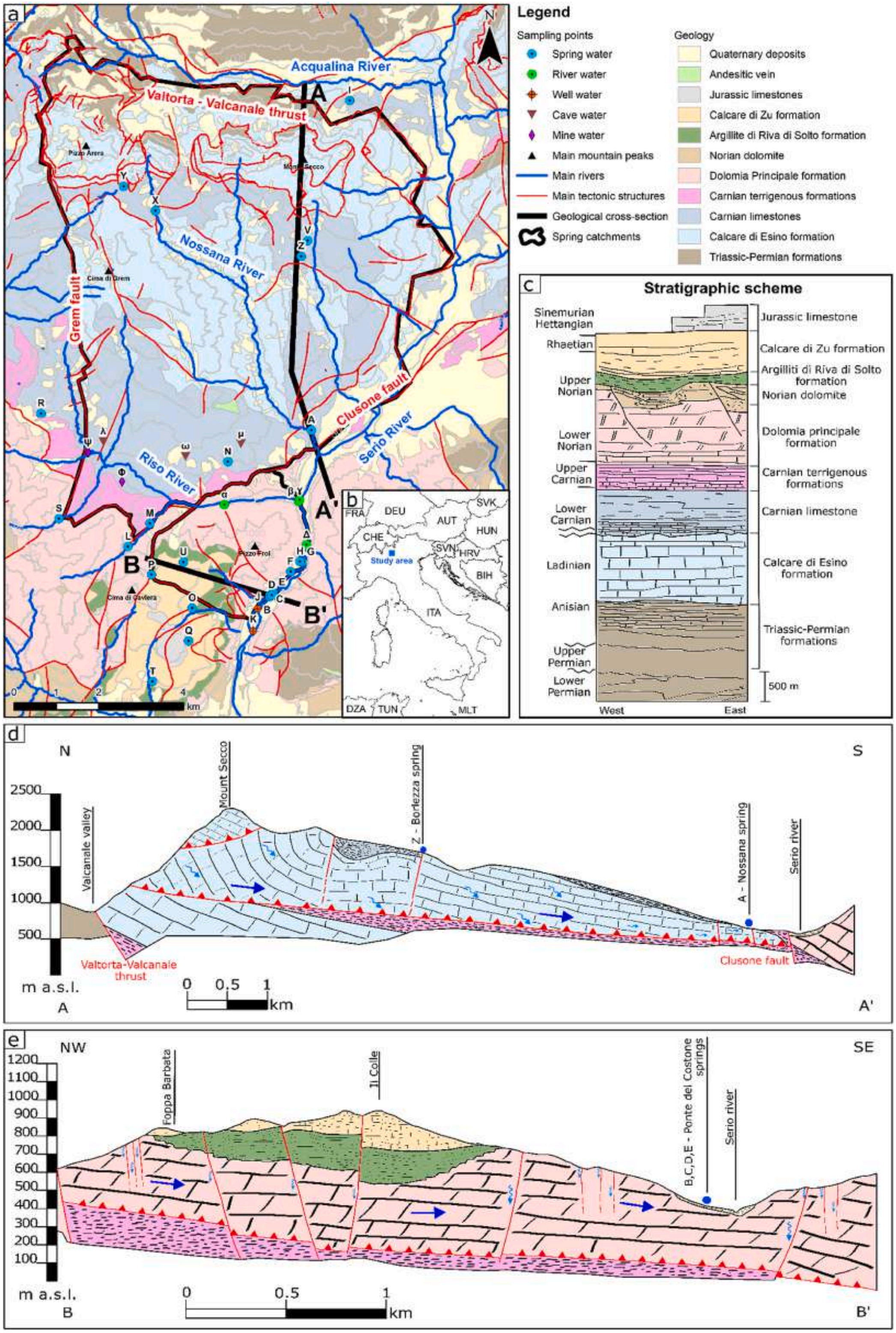

Fig. 1. a) The geological setting, b) the location within southern-central Europe, and c) the simplified stratigraphic scheme of the study area. Also, the d) AA' and the e) BB' geological cross-sections related to Nossana and Ponte del Costone catchments are displayed. Refer to Table 1 for spring ID codes.

3. Methods

3.1. Sampling

Water sampling and monitoring activities focused primarily on the main springs of the Nossana and Ponte del Costone (Galleria del Costone group). They were sampled monthly over one year from May 2018 to July 2019. To characterize the two hydrogeological catchments from the chemical-physical point of view, it was decided to sample some minor springs adequately distributed in space to cover the whole study area, focusing on the border area between the two basins.

A total of 34 sampling points were set up (Fig. 1 and Table 1). Twenty-three points are related to natural spring waters, four to surface waters, two to wells at the valley floor, three to waters deriving from karst caves, and two to the Val del Riso mine winze. Sampling consisted of two main phases: monthly monitoring of the Nossana and Ponte del Costone main springs (five points taken monthly) and an overall sampling at all points once per year (May 2018 and July 2019). Before water sampling, the physical-chemical parameters (namely pH, RedOx potential, electrical conductivity, and temperature) were measured using a multiparameter probe.

In addition, samples were collected during the September 2015 and July 2019 monitoring campaign for groundwater dating with the $^3H/^3He$ method. Five natural springs were sampled for tritium and helium isotopes during a period of low discharges, approaching the baseflow level: Nossana (474 m a.s.l.), Costone 2 (430 m a.s.l.), Valle Rogno (710 m a.s.l.), Camplano (1840 m a.s.l.), and Valmora (1770 m a.s.l.). Only these springs, among the 23 considered for hydrochemical analyses, allowed sampling of gases dissolved in groundwater, i.e., presented conditions suitable for preventing exchanges of gases between groundwater and atmospheric air. A specific survey was carried out to recognize the springs whose characteristics were favorable for $^3H/^3He$ sampling. The noble gas sampling was performed by inserting the polypropylene tubing of the submergible pump into water-filled rock fractures characterized by constant groundwater flow, to ensure laminar flow and avoid contact with external air. The sample was then collected in a copper tube, in which it was shipped to the laboratory. Samples were collected in 2015 and 2019, except for the Valmora spring, which was not included in the 2019 campaign.

3.2. Hierarchical clustering classification

Chemical analyses were performed via ion chromatography (IC) and inductively coupled plasma mass spectrometry (ICP-MS). The main cations (Ca^{2+}, Mg^{2+}, K^+, and Na^+) and the main anions (HCO_3^-, Cl^-, NO_3^-, and SO_4^{2-}) were analyzed for statistical treatment. To further characterize the geochemistry of the water, other important parameters, namely total alkalinity ($CaCO_3$), electrical conductivity, and pH, were analyzed.

The hierarchical cluster analysis method has been widely used in environmental and hydrochemical characterization studies (Déri-Takács et al., 2015; Güler and Thyne, 2004; Helstrup et al., 2007; Zhong et al., 2022). This analysis allows grouping experimental units in classes according to similarity criteria, i.e., to determine the number of classes so that observations within the classes are as homogeneous as possible and inter-classes are as inhomogeneous as possible. The homogeneity is evaluated using a Euclidean distance as a discriminating factor: the smaller the distance between two groups, the greater the similarity. Conversely, parameters with more significant dissimilarity are separated into clusters, according to the methods explained in Davis (1986) and Swan and Sandilands (1995). The selection of these classes was made by application of the furthest neighbor method in which the most prominent dissimilarity between two points in two different clusters is exploited. These division methods start with all objects in one cluster and then split them into smaller clusters until there is one object per cluster according to the investigated characteristics. The hierarchical clustering process results graphically in a tree-like diagram called "dendrogram". In this study, the hierarchical cluster analysis was performed on the spring waters using the software "Instant Clue" (Nolte et al., 2018), and considers the major cation and anion concentrations (Ca^{2+}, Mg^{2+}, K^+, Na^+, HCO_3^-, Cl^-, NO_3^-, and SO_4^{2-}) resulted from the chemical analyses.

3.3. $^3H/^3He$ analysis

In the 2018–2019 biennium, tritium samples for monitoring the monthly activities of three springs (Costone, Sottoplatea, and Nossana) were analyzed by liquid scintillation counting (Janković, 2018; Santoni et al., 2021) at Avignon University. Moreover, in the summer campaigns of 2015 and 2019, the ^3H samples from springs were analyzed by mass spectrometry using the ^3He ingrowth method at the University of Bremen (Sültenfuß et al., 2009). The total concentrations of ^3He, ^4He, and Ne were also measured in all samples collected for $^3H/^3He$ age determination at the University of Bremen. Several studies explain the method in detail (Ekwurzel et al., 1994; Schlosser et al., 1988; Sültenfuß et al., 2009; Tolstikhin et al., 1969).

To correct air excess of noble gas partial pressure (Freundt et al., 2013), the solubilities of He and Ne were calculated in function of equilibrium atmospheric pressure (p_{atm}) and temperature (T_{atm}) using the experimental data of Weiss and Kyser (1978). The values of p_{atm} and T_{atm} were computed as a function of the average altitudes of the recharge area for each spring, assumed to be the mean elevation between the spring altitude and the highest altitude in the catchment (the Arera mount peak). The equilibrium air pressure p_{atm} was then calculated using the standard "exponential atmosphere" barometric formula (NOAA, NASA, USAF, 1976):

$$p_{atm} = exp(\ -M_{air}\ g\ H\ /\ R\ /\ T_{sl}) \quad (1)$$

Where M_{air} is the molar mass of air (0.02897 kg/mol), R is the gas law-constant (8.31454 j/K/mol), g is the acceleration of gravity (9.81 m/s^2), T_{sl} is the standard air temperature at sea-level (288.15 K at p = 1013 hPa), and H is the average altitude of the recharge area (m a. s. l.) calculated as a simple mean between the altitude of the spring and the altitude of the highest mountain peak in the recharge area. This relation gives comparable results to those calculated with another experimental expression given by Beyerle (1999) for the Swiss Alps.

The equilibrium air temperature T_{atm} was then calculated in function of the average altitude H using the classical lapse-rate expression:

$$T_{atm} = A\ \ T_{sl}\ H \quad (2)$$

where A, A is the factor in the formula and T_{sl} and H represent the same parameters as explained before. The value of the lapse-rate coefficient A depends on many factors, which are relatively specific and vary with the local conditions (season, moisture content, topography, soil, vegetation covers, etc.). Since a precise knowledge of the value of this coefficient for the study area is lacking, the standard, A value of 6.49E-3 °C/m, was applied, as done in other studies where a first approximation of this coefficient is considered sufficient for the goals of the research (Barry and Chorley, 2009). The value of equilibration temperature and pressure to calculate the He–Ne solubility, necessary for the model, could be better estimated knowing the actual temperature variation with altitude and the distribution of precipitation in the different seasons in this mountain area.

The excess-air corrections for the sampled waters were determined using the measured Ne-excess in the samples and the standard He/Ne air ratio. The radiogenic ^4He component in the samples was computed by subtracting from the total measured ^4He the calculated He solubility at the average recharge altitude and the He air excess obtained using the Ne excess and the Ne/He of air. The value of the $^3He/^4He$ for the radiogenic component was assumed to be 2E-08 (Mamyrin et al., 1984).

Finally, the tritiogenic ^3He component was obtained from the total measured ^3He, subtracting the contributions of ^3He solubility in water at the average temperature of the recharge area and the He-excess air. The solubility of ^3He is obtained using the standard $^3He/^4He$ ratio of air (1.384E-6) and the standard water-to-air isotopic fractionation $^3He/^4He$ in equilibrium condition:

$$\delta^3He = -1.8 + 0.0084\ T_{atm} \quad (3)$$

where T_{atm} is the temperature calculated from the average altitude of the catchment (eq. 2). The excess air ^3He component was calculated assuming the incorporation of unfractionated dry air, using the excess-

Ne and the He/Ne ratio, as done for the $^4He_{rad}$. Due to the high seasonal variability depending on precipitation and its nature, to account for the result uncertainty, these calculations were repeated by varying the recharge temperature by ±1 °C and keeping the average lapse-rate and the mean recharge elevation values equal to the previous step.

4. Results and discussion

4.1. Hydrochemical groups

The average hydrochemical signatures of all sampled waters (locations shown in Fig. 1 and Table 1) are shown in Table 2. The analyzed waters are summarized in Spring, River, Wells, Karst Caves, and Mine waters. The results of the chemical analyses are presented in full in Table A1 (Appendix A).

Most of the waters are within the magnesium-bicarbonate hydrochemical facies, except for the point at the Riso/Serio confluence (sampling point β) (enrichment in Na^+, K^+, and Cl^-, Sodium – Chloride type) and the Mine waters (with high SO_4^{2-}, Calcium chloride type) (Piper, 1944) (Fig.A1 - Appendix A). Furthermore, a progressive enrichment in Sulfates is observed from north to south for the Ponte del Costone springs (from 3.5 mg/l of the Bosco spring to 48.3 mg/l of the Costone 7 spring).

Hierarchical clustering analysis yields the dendrogram shown in Fig. 2. Three major classes are identified at the Euclidean distance of 60. The average concentration in major ions of the three groups are shown in Table 3. The C (1) class represents the springs having the lowest concentration values in major cations and anions. This group mainly gather the springs at the highest elevations (mean value 1242 m a.s.l.) of the Nossana spring catchment. The C (2) class represents the waters sampled in the Galleria del Costone area (Costone 1, Costone 2, Costone 4, and Costone 7 springs). These waters display the highest contents for every ion investigated (Ca^{2+}, Mg^{2+}, K^+, Na^+, HCO_3^-, Cl^-, NO_3^-, and SO_4^{2-}). The springs constituting the C (3) class are characterized by intermediate values in ion content and correspond to the springs distributed around the Ponte del Costone basin at moderate altitudes (mean value 715 m a.s.l.). From the chemical point of view, point N (Valle Rogno) falls in class C (3), but it is representative of only 9% of the samples in the group. From the geological point of view, it should belong to class C (1). This represents an exception that does not invalidate the reasoning.

The spatial distribution described above is illustrated in Fig. 3. It represents the effect of the main drivers regulating the chemical composition of water in karst carbonate environments: geology, rate of karst development, and elevation (Chemseddine et al., 2015). Their importance relies on the timing and mode of water-rock interaction as well as on the form and quantity in which the chemical elements can be found in rocks.

4.2. $^3H/^3He$ data

Table 4 summarizes the results of the $^3H/^3He$ analysis for waters sampled in September 2015 and July 2019. The comprehensive results of this analysis are reported in Table A2 (Appendix A).

The results of the He–Ne analysis are displayed in Fig. 4, together with an abacus of He–Ne limiting solubilities in the function of p_{atm} and T. The black dotted line in this figure represents the calculated He–Ne solubilities following the P-T altitude gradient as obtained using the barometric exponential formula (eq. 1) and the lapse-rate expression (eq. 2). The upper end of this solubility line indicates the He–Ne solubilities corresponding to the lowest possible altitude of recharge area in the valley (475 m). By increasing altitudes (and consequent p_{atm}-T decrease), He–Ne solubilities decrease following the black dotted line according to the equations of Weiss and Kyser (1978). The lower end of the blue dotted line corresponds to the He–Ne solubilities reached near freezing-point conditions, i.e., at an altitude of about 2317 m. This altitude corresponds to the maximum altitude having an annual average temperature higher than the freezing point, and therefore it represents the maximum altitude of the recharge area "visible" by the $^3H/^3He$ method. The grid of thin light-blue and grey solid lines defines the full range of possible solubility concentrations of He–Ne given the combinations of possible temperature (T) and recharge elevations (H). The dotted lines indicate the most likely solubilities of He–Ne based on the assumed rate of change of recharge T (namely, the most likely recharge H-T combinations). The other two dashed lines in Fig. 4 (purple and lilac lines) represent the Ne–He concentrations in waters having incorporated different amounts of un-fractionated dry air at the moment of recharge, based on the elevation of the recharge area. The slopes of these lines are defined by the Ne/He ratio of the un-fractionated dry air (0.288). In the absence of a radiogenic contribution, the He–Ne solubility concentrations of sampled waters lie within the area of influence defined by these two lines.

The initial ^3H calculated from the presented $^3H/^3He$ data of all springs, i.e., the sum of ^3H still present in the sample and the tritiogenic ^3He produced by the decay of tritium initially present in the sample, are illustrated in Fig. 5, together with the ^3H record in precipitations at Vienna (taken from the database of IAEA - Atomic Energy Agency (https://nucleus.iaea.org/wiser/)).

Fig. 6 shows the resulting recharge ages and initial tritium units of spring waters assuming the given altitudes of recharge (blue dots). The effects of recharge temperature variations of ±1 °C are also plotted for two limiting cases. The squares represent ages and initial ^3H assuming

Table 1
Sampling points, their types, their altitudes (only for spring waters), and their identification codes (IDs) in agreement with those shown in Fig. 1.

ID	Name	Type	Altitude (m a.s.l.)	ID	Name	Type	Altitude (m a.s.l.)
A	Nossana	Spring	482	R	Spiglello	Spring	970
B	Costone n.1	Spring	423	S	Val Noseda	Spring	822
C	Costone n.2	Spring	423	T	Piazza Rivolta	Spring	687
D	Costone n.4	Spring	423	U	Caalù	Spring	953
E	Costone n.7	Spring	423	V	Fontana Calda	Spring	1653
F	Merlo	Spring	438	X	Valmora	Spring	1770
G	Sottoplatea	Spring	428	Y	Camplano	Spring	1840
H	Bosco	Spring	439	Z	Borlezza	Spring	1575
I	Val Las	Spring	917	α	Riso Upward	River water	–
J	Costone n.4	Well	–	β	Confluence Riso/Serio	River water	–
K	Costone n.2	Well	–	γ	Serio Upward	River water	–
L	Musso	Spring	679	Δ	Serio Downward	River water	–
M	Spino	Spring	634	Ψ	Discenderia Firenze	Mine water	–
N	Valle Rogno	Spring	699	Φ	Discenderia Selvatici	Mine water	–
O	Val Preda	Spring	862	λ	5 Cascate Cave	Karst cave	–
P	Berlina	Spring	996	ω	Battista Moioli Cave	Karst cave	–
Q	Fontana del Lacc	Spring	923	μ	Gibelì Cave	Karst cave	–

Table 2
The maximum, mean, and minimum values for the abundance of major cations and anions for each collected type of water are expressed in mg/l.

Sampled waters	Ca^{2+} [mg/l]	Mg^{2+} [mg/l]	Na^{+} [mg/l]	K^{+} [mg/l]	HCO_3^- [mg/l]	Cl^- [mg/l]	NO_3^- [mg/l]	SO_4^{2-} [mg/l]
Min values	29.0	1.2	0.5	0.3	129.7	1.0	2.0	1.5
Average springs (23 samples)	53.3	13.9	3.7	1.5	199.2	1.4	4.1	10.4
Max values	74.4	20.8	6.5	3.0	247.8	12.9	7.3	50.4
Min values	27.3	6.2	2.1	0.9	87.5	2.6	3.4	12.1
Average rivers (4 samples)	48.5	10.6	35.2	28.8	140.2	81.4	5.2	31.5
Max values	73.9	14.1	116.2	98.2	193.0	249.2	6.1	63.0
Min values	53.8	20.6	1.0	0.5	222.0	2.0	4.0	13.0
Average wells (2 samples)	60.0	21.6	3.0	0.7	242.5	2.5	5.0	13.0
Max values	66.2	22.7	5.0	0.9	263.0	3.0	6.0	13.0
Min values	47.4	5.5	1.5	0.4	159.0	2.0	4.0	7.5
Average Karst caves (3 samples)	58.3	21.5	2.7	0.5	185.2	4.5	5.0	9.5
Max Values	68.9	10.1	4.5	0.6	214.0	9.5	5.5	11.0
Min values	105.7	20.0	3.0	0.8	145.5	3.0	2.0	215.5
Average Mines (2 samples)	114.2	22.4	3.2	0.9	146.2	3.2	2.5	253.7
Max values	122.7	24.8	3.5	1.1	147.0	3.5	3.0	292.0

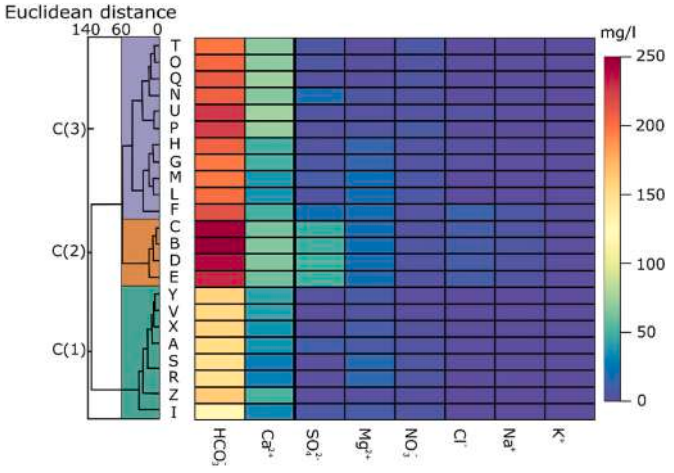

Fig. 2. Summary dendrogram of the Hierarchical clustering analysis. Refer to Table 1 for the ID codes of the springs.

that temperature variations occur at the same recharge altitude (same equilibrium partial pressure, Table 4). The diamonds represent instead ages and initial ^3H assuming that temperature variations of ±1 °C are the result of changes in recharge altitude. In this case, changes of gas solubilities as a response to equilibrium temperature and partial pressure (which vary according to the altitude, i.e., eqs. 1 and 2) partially offset each-other, so the resulting shift in calculated ages is lower than the previous case. Therefore, ages of the high-altitude springs slightly vary, but the age-relationships between springs remain the same. In other words, they change equally but not one in comparison to each other.

To evaluate the mean ^3H in the catchment, tritium activity was also analyzed for other springs and rivers in the study area (in Table A2, Appendix A). Tritium samples in the catchment returned relatively homogenous activities, with an average of 5.1 TU, very close to the average activity observed at the main springs Nossana and Ponte del Costone. Average tritium activity in river waters (5.3 TU) is also very similar to the one measured in the springs. The five springs sampled for $^3H/^3He$ data may be subdivided into three groups based on the "Estimated Recharge elevation" column of Table 4: the high-altitude springs (Valmora and Camplano), the intermediate-altitude springs (Nossana and Valle Rogno), and the valley bottom spring (Costone 2). The main differences found between the groups are.

i. High-altitude springs contain a limited excess of air and a low radiogenic ^4He, consistent with their young $^3H/^3He$ ages (0–2 years).
ii. The intermediate-altitude springs contain substantially more excess air than the high-altitude springs. They exhibit low radiogenic ^4He content, consistent with their intermediate ages (4–13 years). The 2019 Nossana samples are consistently older than the rest of the group (12–13 years compared to 4–7 years).
iii. The low-altitude springs also have a high air excess, similar to that of the intermediate-altitude springs. They have the oldest $^3H/^3He$ ages (29–32 years) and a higher radiogenic ^4He than the intermediate-altitude springs.

The following sections briefly discuss the specifics of these groups.

4.2.1. *The high-altitude springs*

The measured He–Ne concentrations of these springs are close to the He–Ne solubilities predicted for the average recharge altitude, following the local altitude gradient (blue dotted line in Fig. 4). However, the equilibration altitudes corresponding to the measured He–Ne concentrations result much lower than the actual altitude of these springs (data in Table 1). These lower, apparent equilibration altitudes are probably the result of a minor He–Ne air excess present in these samples: $\Delta Ne = 3.1\%$ for Valmora spring and ΔNe included between 4.8 and 6.3 % for Camplano spring. This minor, almost constant air excess is possibly

Table 3
The average values for the abundance of major cations and anions for the groups obtained with the application of the Hierarchical clustering analysis, expressed in mg/l.

Water classes	Ca^{2+} [mg/l]	Mg^{2+} [mg/l]	Na^{+} [mg/l]	K^{+} [mg/l]	HCO_3^- [mg/l]	Cl^- [mg/l]	NO_3^- [mg/l]	SO_4^{2-} [mg/l]
C (1) (8 samples)	37.7	9.0	0.6	0.3	150.2	1.0	3.9	3.6
C (2) (4 samples)	63.5	19.9	4.9	1.3	240.6	9.4	5.1	48.9
C (3) (11 samples)	58.7	9.6	1.6	0.8	207.7	2.8	5.4	7.8

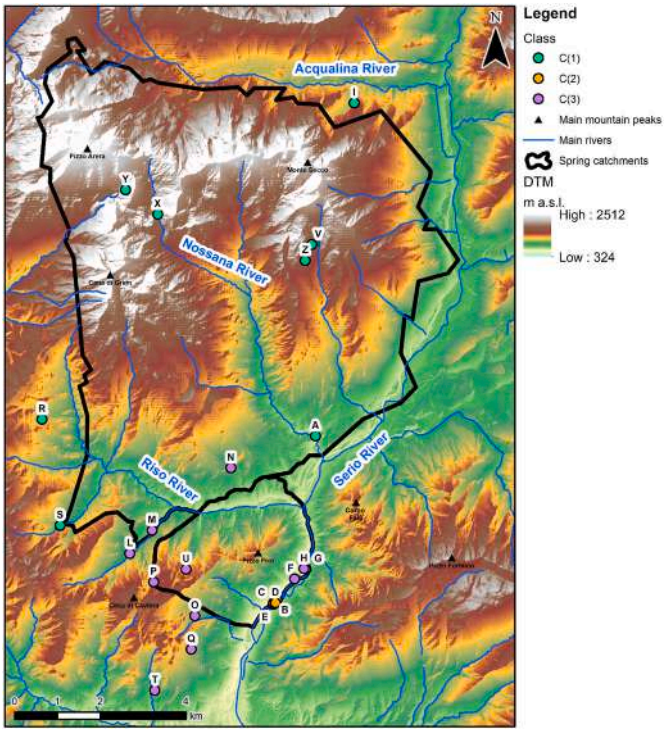

Fig. 3. Spatial distribution of sampling points, divided by classes as obtained from the Hierarchical clustering analysis for the Nossana spring catchment (North) and the Ponte del Costone basin (South).

related to groundwater recharge processes occurring through shallow unconsolidated material before entering fractured limestones and dolostones (Manning et al., 2021). At high elevations, the recharge area can be characterized by outcropping bedrock with open fractures as well, therefore other possible sources of the small excess air cannot be excluded a priori and should be investigated in further studies. No radiogenic ^{4}He component was detected in these springs in 2015 and 2019.

Tritium samples collected in 2019 returned activities similar to those measured in 2015. The tritiogenic ^{3}He component is very low for these springs, so the computed ^{3}H/^{3}He ages (Table 4) result "young", particularly for the 2015 sample from the Camplano spring. The low ^{3}He concentrations of these samples, and particularly their low tritiogenic ^{3}He component, are consistent with a recharge area situated at high altitude, likely leading to short groundwater residence time, given the karstified nature of the aquifer formation. An apparent slightly older age is observed for Camplano spring in 2019 (1.8 y) in respect to the 2015 sample (0.2–0.7). However, this minor age-difference for the same spring is considered smaller than the typical age resolution of the 3H/3He method (±1–2 years, Visser et al., 2014).

Fig. 5 shows that these two high-altitude springs yield initial ^{3}H values close to the range of ^{3}H levels of the precipitations recorded at Vienna IAEA at the calculated ^{3}H/^{3}He ages, suggesting that the samples do not contain pre-modern waters, as expected from the lack of radiogenic ^{4}He, the young ^{3}H/^{3}He ages and the high-altitude recharge area. Although tritium seasonal fluctuations in precipitations may vary over a regional scale (Vienna tritium record is obtained about 600 km away from the sampled spring) and mixing of seasonal inputs may also differ with time, data show that high altitude springs yield initial ^{3}H close to the lower limit of the Vienna ^{3}H record (recharge during fall) while the low altitude springs tend to fall on the upper ^{3}H range (recharge during spring). This difference may thus suggest a local seasonal effect on the main recharge mechanism and should be further investigated in future studies.

4.2.2. *The intermediate-altitude springs*

Nossana and Valle Rogno are characterized by a significant He–Ne air excess (ΔNe = 29.5–43.9 %), which could be mainly due to large fluctuations of the water table in the karstic formations (e.g., Manning et al., 2021). Water flow rates at Nossana spring are observed to respond rapidly to rainfall inputs (Citrini et al., 2020), likely indicating that within the Esino limestones the water-table may vary significantly. A recharge through porous soil could also contribute to the excess air, since the gas contained in the soil porosity may easily be trapped in water as small bubbles during the groundwater recharge process (Andrews, 1992; Beyerle, 1999; Osenbrück, 1991). The soil thickness is generally higher at lower altitudes than at high altitudes, which is consistent with the data available from the Regional Agriculture and Forestry Agency database (ERSAF, 2010), indicating soil thickness ranging from 2 m at the valley bottom to about 20 cm around the Mt. Arera peak.

In Fig. 4, the 2019 Nossana samples lie close to the air-excess line plotted for water recharged at 475 m. This altitude cannot, however, represent the mean recharge altitude of the spring, as the spring represents the base level of the catchment. Any recharge altitude between 475 and 2512 m a.s.l. can explain the He–Ne excess provided that a ^{4}He radiogenic component is present in these 2019 samples. The 2015 Nossana and Rogno samples lie instead on the upper limiting excess-air line, indicating an absence of a radiogenic component. The higher Ne concentration in the 2015 than in the 2019 samples for Nossana and Val Rogno may be the combination of several factors: i) a higher altitude of recharge in 2015, implying an initial He–Ne equilibrium concentrations plotting close to the high altitude, upper dashed-line; ii) a lower initial He–Ne equilibrium temperature at the moment of recharge in 2015, which also has the effect of increasing the Ne equilibrium concentration

Table 4
Summary of the ^{3}H/^{3}He sampling results conducted in September 2015 and July 2019.

Sample ID	Estimated recharge elevation	Sampling date	^{3}H	^{3}He/^{4}He	ΔNe	Δ^4He_{rad}	$\Delta\ ^3He_{tri}$	Apparent Age	Recharge time	"Initial" tritium
	[m a.s.l.]		[TU]		[%]	[%]	[%]	[years]		[TU]
A –Nossana	1493	Sep-15	5.6 ± 0.2	1.5E-06	43.4	0.0	55.7	6.5	2009.3	8.1
			5.6 ± 0.2	1.5E-06	42.5	0.0	54.5	6.1	2009.7	8.0
		Jul-19	5.4 ± 0.4	1.6E-06	41.7	2.3	53.6	12.5	2007.1	10.8
			5.4 ± 0.4	1.6E-06	44.6	2.3	57.2	12.8	2006.8	11.0
C –Costone 2	765	Sep-15	5.5 ± 0.2	2.0E-06	39.7	19.5	49.6	29.6	1986.1	29.0
		Jul-19	4.7 ± 0.4	2.0E-06	39.7	21.7	49.6	32.4	1987.3	29.1
N –Valle Rogno	1611	Sep-15	4.8 ± 0.2	1.5E-06	37.9	0.0	48.8	6.7	2009.1	7.0
		Jul-19	4.8 ± 0.8	1.4E-06	29.5	0.0	38.0	4.3	2015.4	6.1
			4.8 ± 0.8	1.5E-06	35.5	0.0	45.8	5.4	2014.2	6.5
X –Valmora	2186	Sep-15	5.5 ± 0.2	1.4E-06	3.1	1.7	4.0	1.7	2014.1	6.0
Y –Camplano	2176	Sep-15	5.4 ± 0.2	1.4E-06	4.8	0.0	6.3	0.2	2015.6	5.5
		Jul-19	5.8 ± 0.4	1.4E-06	5.8	1.6	7.6	1.8	2017.9	6.4

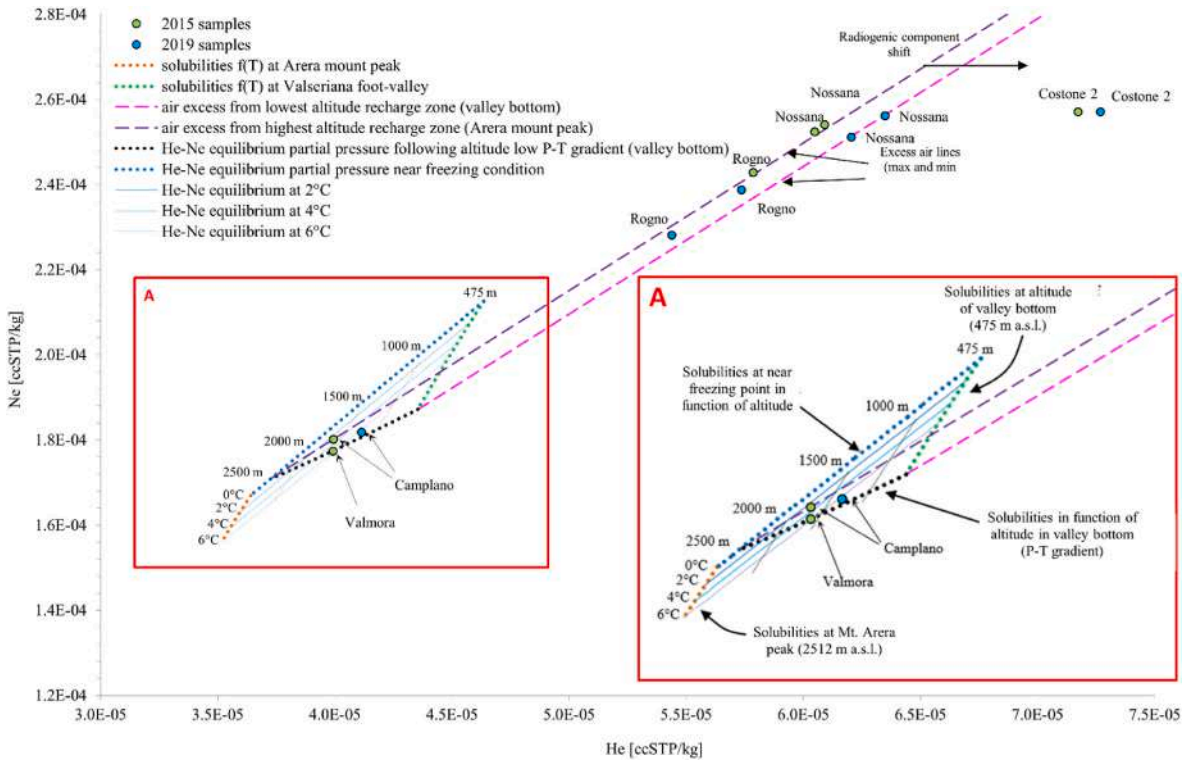

Fig. 4. He–Ne relation of the sampled waters according to Table 3. The green dotted line represents solubilities following the pressure-temperature altitude gradient. The blue dotted line indicates He–Ne solubilities at near-freezing conditions in function of altitude. The two dashed lines show Ne–He concentrations trends due to incorporating unfractionated dry air. The zoom of the field of possible noble gas partial pressure at the moment of recharge in the catchment is shown in box A.

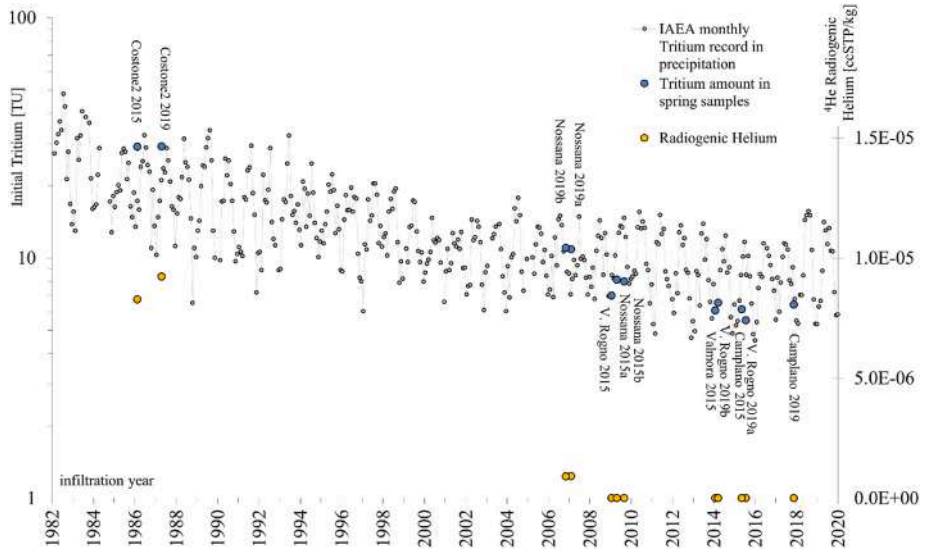

Fig. 5. Initial ^{3}H (blue dots, left Y axes) and radiogenic ^{4}He (yellow dots, right Y axes) in spring samples. The ^{3}H record in precipitations measured at Vienna is shown for comparison.

in respect to the He slightly; iii) the presence of small radiogenic ^{4}He components for the 2019 samples, for both Nossana and Val Rogno, which has the effect to shift the representative point of these samples to the right in Fig. 5.

The three samples of Val Rogno returned similar ^{3}H activities and $^{3}H/^{3}He$ ages of around 5–6 years. Nossana spring also yielded similar age in 2015 (6.3 years) but a significantly older age in 2019 (12.7 years). The infiltration year of the sample collected in 2019 (mean recharge date around 2007) thus anticipates the one of 2015 (mean around June 2009). These older $^{3}H/^{3}He$ ages are consistent with detecting a minor though measurable radiogenic $^{4}He_{rad}$ component in the 2019 sample (Table 4). The initial ^{3}H measured at Nossana in 2019 is also clearly higher than the one found in 2015, and it approaches the yearly average tritium precipitation record of Vienna at the calculated recharge time (Fig. 5). This difference in the initial ^{3}H in the 2015–2019 samples may result from variable mixing and homogenization processes of water inputs during groundwater flow probably driven by variable discharge (see Fig.A2).

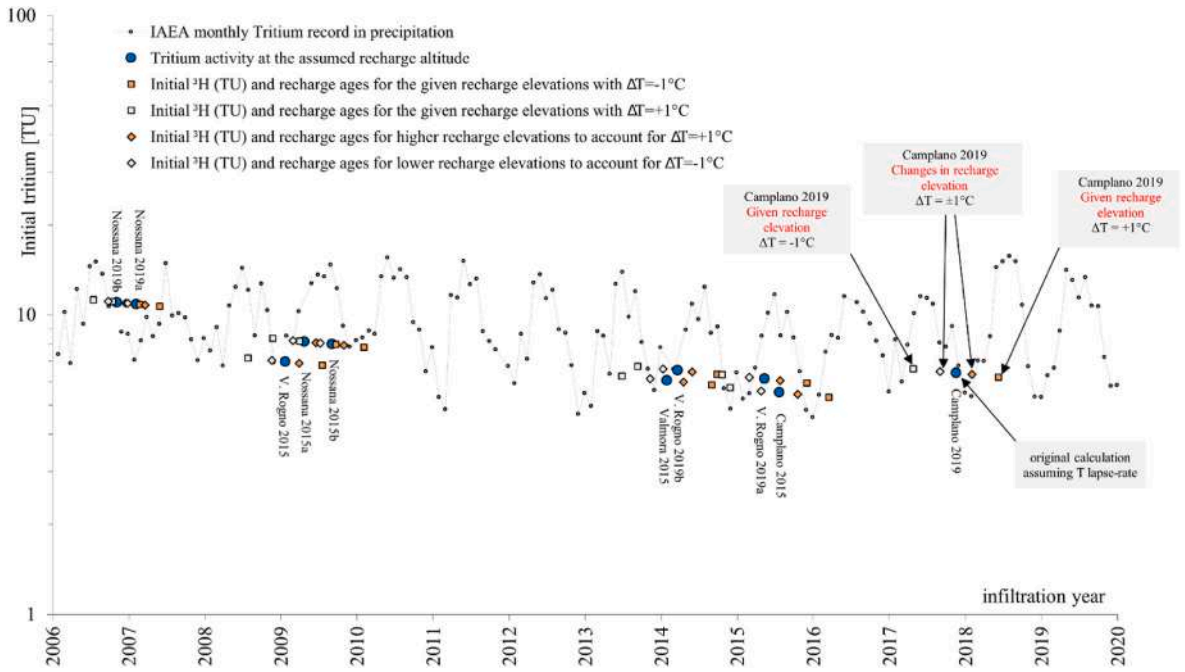

Fig. 6. Calculated recharge ages and initial ^{3}H (TU) of Valseriana springs. Blue dots are calculated assuming the given recharge altitude (Table 2); grey and orange squares are obtained by varying the recharge temperature by ±1 °C at the given recharge altitude (Table 4); grey and orange diamonds are obtained by varying the recharge altitude to account for recharge temperature variation of ±1 °C.

4.2.3. *The valley bottom springs*

For the Costone 2 spring, a significant radiogenic component was detected in both samples of 2015 and 2019. An important amount of air excess is also present in these samples, similar to the one observed for Nossana. In Fig. 4, the presence of the radiogenic component determines a clear shift of these samples to the right of the excess-air lines, particularly for the 2019 samples. The presence of radiogenic ^{4}He is also consistent with the older ^{3}H/^{3}He ages of this spring (at the limit of the age resolution of the ^{3}H/^{3}He method) to 2015 campaign (Table 4, 29.6 years in 2015, increasing to 32.3 years in 2019). The recharge "dates" of these spring waters (1986 and 1987) thus are remarkably similar for the two samples. The initial ^{3}H measured in these samples (Fig. 5) is close to the highest ^{3}H activities of the Vienna precipitation record (1986 and 1987). Assuming that the ^{3}H Vienna record is representative of the precipitation in this sector of the Alps, the calculated initial ^{3}H of the Nossana spring suggests that the recharge of these waters occurred dominantly at the end of springtime, while the high-altitude springs would represent a recharge with contributions in different seasons. As for the other springs, mixing with old 3H-free waters is unnecessary to explain the ^{3}H/^{3}He data. The radiogenic component may thus be described by the ^{4}He generated by the alpha-decay of U and Th and their daughter nuclides in the aquifer during the transit time of this water in water-saturated conditions. The ^{4}He ingrowth rate computed using the Costone 2 data resulted equal to 2.8E-7 ccSTP/kg/y, which is an ingrowth rate lower than that obtained in other studies (Gil-Márquez et al., 2020; Kaown et al., 2009). As an example, in a recent ^{3}H/^{3}He study on very young groundwater samples of a Triassic Mueschelkalk aquifer (Upper Rhine Plain), Moeck et al. (2021) found more significant ingrowth rates of about 8.6E-6 ccSTP/kg/y.

Fig. 7 illustrates the tritium time records, obtained with Liquid Scintillation Counting (LSC) (Horrocks, 2014; Varlam et al., 2009), for the three main springs in the lower part of the valley: Nossana, Costone 7 and Sottoplatea (Costone 7 is a spring few meters away from Costone 2 spring, both being part of the same system). Despite the larger analytical uncertainties of the LSC technique compared to the ^{3}H/^{3}He method, all records show measurable fluctuations of tritium activities and a slightly decreasing trend of ^{3}H with time. Standard statistical technique as the Mann Kendall test indicates that this decrease in time is statistically significant at least for the Costone 7 spring ($p = 0.022$, $tau = -0.49$) and results on the same order of magnitude of the ^{3}H decay rate (apparent half-lives of 4.44 for Costone 7).

^{3}He levels in Nossana are generally higher than in Costone 7 and Sottoplatea. ^{3}H fluctuations for Nossana are also more prominent than the ones observed in Costone 7 and Sottoplatea, with a peak activity of 7 TU reached in November 2018. This variability suggests the episodic presence of a shorter residence-time water component in Nossana spring, compared to Costone 7 and Sottoplatea. Also, it can be noted that the tritium measured in Nossana using the ^{3}He–^{3}H method for the September 2015 sample (5.6 ± 0.2 TU, Table 3) is identical, within errors, to the value obtained in September 2018 using LSC (5.4 ± 0.3 TU, Fig. 7).

4.3. *Conceptual model*

Fig. 8 represents the conceptual model coherent with the results presented in the previous sections. Two different models are proposed: one for Nossana and one for Ponte del Costone. The evidence derived from the analyses conducted in this study led to defining the processes and mechanisms of the two main flow systems of Nossana and Ponte del Costone in a hierarchical model, as described by Asante et al. (2018), echoing the general concepts of White (2002). The two systems are dynamically controlled by the amount of precipitation recharge and the associated piston effect, but with different timing: diffuse infiltration and dripping circulation for the C (2) spring group limit the seasonal variability of discharge rate and favor mixing of different contribution (Fig. 8). Conversely, the dominant drainage system that characterized the C (1) and C (3) groups favors the rapid response of the springs as well as a significant seasonal variability in discharge. The latter accentuates groundwater mixing processes and could explain the different ^{3}H/^{3}He ages between the two sampling campaigns. Diffuse infiltration of precipitation water recharges the karst aquifer system through the soil. Still, the dynamics with which it circulates in the two water systems are governed by the response to the karst dissolution of the encasing rock (Calcare di Esino and Dolomia Principale formations).

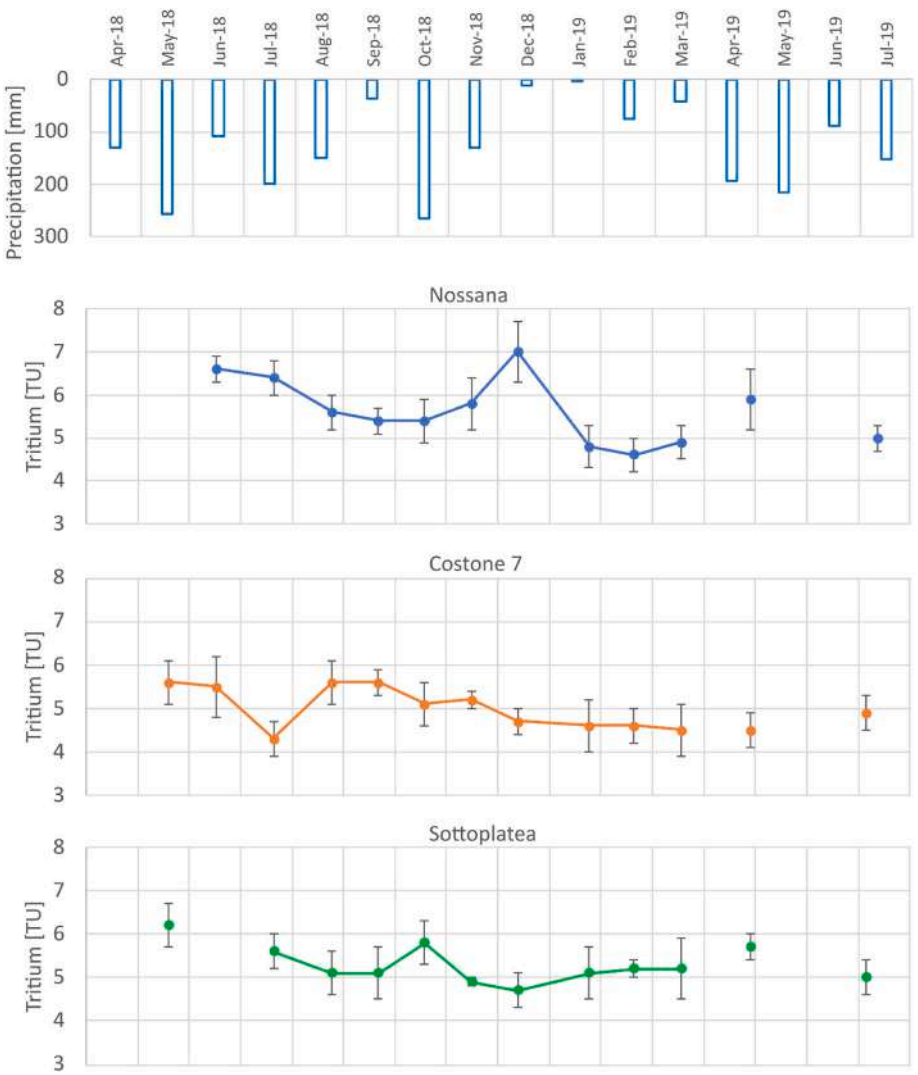

Fig. 7. Time variations (May 2018–July 2019) of tritium concentrations for three main springs sampled: Nossana Spring, Costone 7 spring (some spring system of Costone 2 spring) and Sottoplatea (Bosco area). Also, the monthly cumulative precipitation in mm recorded at the Clusone weather station (4 km from Nossana outlet) are displayed.

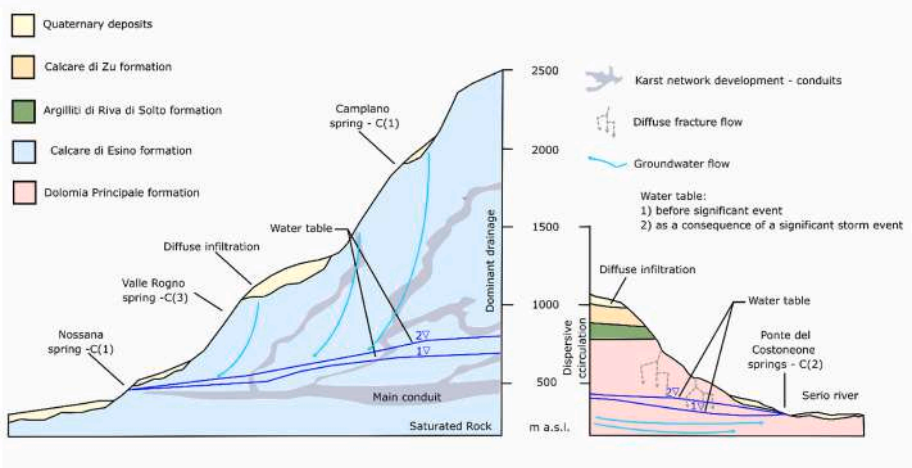

Fig. 8. Conceptual model depicting water circulation in the two karst systems (modified from Asante et al. (2018) and re-elaborated from White (2002)). The model proposed for the Nossana spring is displayed on the left, and on the right, the one for the Ponte del Costone spring system.

In the case of the Ponte del Costone catchment, the relative old age of the Galleria del Costone group is consistent with the relative enrichment in sulphate (average of 48.9 mg/l, compared to the spring water average of 13.3 mg/l). Although the three groups (Galleria del Costone, Merlo, and Bosco) belong to the same water system, they are controlled by families of discontinuities with different persistence (GeoTer, 2000). In the area of the outlet of the springs of the Galleria del Costone, the marked displacement leads to the contact of the waters with a terrigenous formation characterized by the occurrence of chalks. For the Serio River, this structural context results in an enrichment in sulphates from upstream to downstream. This trend is similar to many chemical-physical parameters within the three main areas of the Ponte del Costone springs.

4.4. Discussion

Although analytical uncertainties and assumptions made to calculate air excess may partially justify these differences, all waters sampled in 2019 appear shifted to the right side of the Ne–He air-excess lines in the diagram of Fig. 4, compared to all samples collected in 2015. Possible explanations include.

i. A larger amount of radiogenic 4He component and thus an increased age for the 2019 waters.
ii. A decrease in the mean recharge altitude of the springs in the 2019 samples in respect to 2015 samples.
iii. A larger air excess (e.g., for Camplano samples this possibility could be indicated by the higher ΔNe value measured for the 2019 sample in comparison to the 2015 one).
iv. Sampling issues or analytical errors (e.g., for Val Rogno, 2019, the higher excess air tube could have incorporated a bubble).

In detail, a lower altitude of recharge implies a slightly lower Ne/He solubility ratio and thus a relative increase of He in respect to Ne concentrations at the moment of recharge, which will shift the sample point to the right of the air-solubility line. Longer residence time could result from longer groundwater pathways determined by the larger difference in altitude in the catchment recharge area and, also, from local climatic (inter-annual) variations of the precipitation regimes in the catchment. The possible shifting of the recharge zones to lower altitudes is consistent with the general decrease of snowfall observed in the Central Alps (Matiu et al., 2021; Rumpf et al., 2022). As shown in Fig. 8, higher average altitudes of recharge yield in this setting longer groundwater pathways and so larger transit times.

Noble gas excesses observed in these springs are inversely proportional to the average altitude of the spring's recharge area. The origin of the gas excess has been discussed in many previous papers (Heaton and Vogel, 1981; Herzberg and Mazor, 1979; James et al., 2000; Manning and Caine, 2007; Manning and Solomon, 2003; Top et al., 1987). Given the hydrogeological setting of the studied valley, the observed air excess in spring waters is probably originated or enhanced by the presence of soils in the recharge areas, which are more developed at lower altitudes. During the initial infiltration, soil water entraps small air bubbles in the soil porosity due to surface tension phenomena. The recharge contribution through soil is more significant at lower altitudes than high altitudes, mainly through open rock fractures. So, waters recharged through soils at lower altitudes should yield larger noble gas excesses. This air enrichment can be related to another process consisting in large fluctuations of the water table in the karst formations. For this reason, the significant noble gas excess observed in the water of Nossana is not consistent with the C (1) group (high-altitude springs).

The 2019 sampling highlighted increased groundwater ages and larger noble gas excess than the 2015 samples for most of the springs. However, only the water aging of Nossana is reasonably certain, since age shifts for the other springs are too small compared to the precision of the dating method (±1–2 years) to be believable. For Costone 7, the tritium activities time record analyzed by LSC shows a statistically significant decrease, which is also consistent with the increasing ageing of the groundwater reservoir for the most recent samples. However, further data would be necessary to verify if this trend is maintained over the years. However, further data is necessary to verify if this trend is maintained over the years and significant at other springs too. Furthermore, the excellent match between the Initial ^{3}H activities found in these springs with the tritium precipitation recorded at Vienna (Fig. 5) suggests that water migration through the aquifer may be represented overall by a piston flow model with limited dispersion and mixing with old groundwater. Although a minor dilution with old ^{3}H-free waters cannot be completely ruled out, the piston flow model assumption is retained the most plausible. On the other hand, a ^{4}He radiogenic component is clearly detected in Costone spring, which points to a significantly longer water residence time of these waters, which also implies an in-situ ^{4}He production rate in the aquifer in good agreement with the values found in other studies (Top et al., 1987; Weiss, 1970, 1971).

Looking at the hierarchical distribution obtained using the geochemical data, we may find three spring classes (Fig. 3) that closely reflect the distinctions made using the tritium – noble gas data. The C (1) class closely corresponds to the high-altitude spring waters having short residence time and low air excess. The C (3) class, compared to the intermediate altitudes springs, also has intermediate residence time and intermediate noble gas excess. Finally, the C (2) class represents the low-altitude spring system of the Costone springs, having a long-residence time and the highest noble gas excess.

The Nossana spring falls in the C (1) class with an intermediate residence time found with the ^{3}H/^{3}He method. This intermediate residence time is consistent with the long groundwater pathway from the high-altitude recharge area to the bottom of the valley. The geochemical signature of this high-altitude spring (C (1)-type) is, therefore, well preserved during this long path. The multiple faults related to the large syncline-fold structure in the Calcare di Esino Formation (Jadoul et al., 1985) represent the main high-altitude recharge area. The presence of rock fractures that typically characterize this formation confers a double permeability to the aquifer, which probably increases the hydraulic dispersion. This effect could explain the variability in time of the ^{3}H activity of this spring (LSC ^{3}H record). There is a need for additional ^{3}H/^{3}He data to verify whether this double permeability feature yields a clear difference in ^{3}H/^{3}He ages.

Regarding hydrodynamics, the estimated water transit times are in a range compatible with the conceptual model of the spring systems. Therefore, the systematic dating of karst groundwater using ^{3}H/^{3}He appears possible, provided that the water sampled for the analysis is not outgassed and of ages not exceeding 40 years (Kazemi et al., 2006). Delbart et al. (2014) and Gil-Márquez et al. (2020) argued against using the ^{3}H/^{3}He method for karst systems, but the reasons mentioned in the study apply strictly to their case (e.g., the proximity of the study area to a nuclear facility or samples collected under different hydrodynamic conditions). In the case of the Valseriana valley, the water mass entering the two spring systems is isolated from the atmosphere once in the saturated zone, and only those springs characterized by favorable sampling conditions were selected to perform the investigation so that the technique led to excellent results (confirmed by repeating the analyses at 4–5 years distance, in 2015 and 2019). These good results point out the importance of direct-observation surveys of potential sampling points to plan a successful campaign. Moreover, in this study, sampling avoiding the degassing of dissolved noble gases was achieved by pumping the water samples directly from rock fractures, so that external air could not affect the sampled waters. It is also possible that the water sampled inside the rock fractures was in contact with the gas trapped in the epikarst or in fractures without exchanges with external air, i.e., in "closed conditions" to gas exchanges. In this trapped air, the noble gas's partial pressures were permanently equilibrated with the constant flow of incoming groundwater, preventing degassing. Insights regarding the

relevant flow and transport parameters for different sections of the aquifer system could be obtained through artificial dye tracer tests as demonstrated by Lauber et al. (2014). However, such tests, although suggested, have never been approved by the company managing the springs for domestic water supply.

5. Conclusions

The study combined Hierarchical cluster analysis with the $^{3}H/^{3}He$ dating method to gain knowledge on the residence time and the hydrodynamics of one of the largest spring systems in the Italian pre-Alps. The main results of this study are highlighted as follows.

- It has been proven that spring water dating by the $^{3}H/^{3}He$ method is feasible in a karst context similar to the study area. The application of this technique was robustly endorsed by repeating the analyses at a distance of 4–5 years and obtaining coherent results. This was achieved by taking water samples before equilibrium with the external air was reached directly from the spring outlet.
- Three groups of springs were defined based on chemical characteristics and residence time: high altitude springs (age less than one year), intermediate altitude springs (age between one and 10 years), and valley bottom springs (age more than 10 years). These differences are not necessarily due to the length of the flow path but rather the difference in the hydraulic transmissivity of the aquifers: the C (2) group is less permeable with dripping circulation, whereas the C (1) and C (3) are characterized by dominant drainage with large conduits (Fig. 8). the valley bottom springs C (2), considering the higher age and exposure to anthropogenic pressures in comparison to C (1) and C (3) groups, gain priority in terms of water resource protection. Besides being an outlier because of the tectonic structure of its catchment (it belongs chemically to the group of high-altitude springs but has residence times of the intermediate category), the Nossana spring has the specificity of providing the highest discharge rates in the area, making its protection crucial for the drinking demand of the entire Province of Bergamo.
- Significant noble gas air excess is generally found inversely related to the spring elevations. In recent samples (2019), the excess air is higher than in older ones (2015), probably indicating a tendency toward lower recharge altitudes, i.e., a recent decrease in snowfall or winter recharges. Stable isotopes ($\delta^{2}H$ and $\delta^{18}O$) also suggest a lower recharge altitude for the Galleria del Costone spring group in comparison to Nossana and other springs in the area.

These findings lead to a better understanding of the two systems work and the residence times of waters that characterize the Valseriana area. The $^{3}H/^{3}He$ results also provided information on the duration of the renewal cycle of the water reservoir and, therefore, on the nature of the spring itself. For these main springs, the cyclical renewal of the resource is not evident; instead, the water reserve becomes older in the 2015–2019 comparison. This leads to the conclusion that recent water fails to renew the whole water storage. further studies including repeated Helium–Neon analyses over a longer time-series could verify this observed trend of increasing ages and reducing recharge altitudes, as well as to better constraining the conceptual model of the study area. This will contribute to better assessing the water mixing and discharge variability (especially for the Nossana) of spring systems, which are particularly rich in consequences for water resource availability and management in the context of future climate change.

All authors have read and agreed to the published version of the manuscript.

Funding

This research was funded by the framework agreement between UniAcque S.p.A. and Dipartimento di Scienze della Terra “Ardito Desio”. In addition, it was partly supported by the Italian Ministry of Education (MIUR) through the project “Dipartimenti di Eccellenza 2023–27” and by the ENeRAG – Excellency Network Building for Comprehensive Research and Assessment of Geofluids project funded by the European Union’s Horizon 2020 research and innovation program under grant agreement No 810980.

CRediT authorship contribution statement

Andrea Citrini: Writing – original draft, Software, Methodology, Investigation, Formal analysis, Data curation, Conceptualization. **Adriano Mayer:** Writing – review & editing, Supervision, Software, Methodology, Investigation, Formal analysis, Conceptualization. **Corrado A.S. Camera:** Writing – review & editing, Supervision, Methodology, Conceptualization. **Anita Erőss:** Writing – review & editing, Supervision. **Jürgen Sültenfuß:** Writing – review & editing, Software, Formal analysis. **Guido Pezzera:** Writing – review & editing, Data curation. **Giovanni Pietro Beretta:** Writing – review & editing, Supervision, Resources, Methodology, Funding acquisition, Conceptualization.

Declaration of competing interest

The authors declare the following financial interests/personal relationships which may be considered as potential competing interests.

Giovanni P. Beretta and Corrado A.S. Camera report that financial support was provided by UniAcque S.p.A.

Data availability

Data will be made available on request.

Acknowledgements

The authors thank UniAcque S.p.A. for their support and all the laboratories involved in the research for their professionalism.

Appendix A

This section provides the results of chemical analyses for each point sampled between September 2015 and July 2019 (Table A1) and a Piper diagram of mean water point values (Fig.A1). Moreover, the results of the $^{3}H/^{3}He$ analysis and variation of tritium content for the Nossana spring waters in relation to the monthly mean discharge and precipitation are shown in Table A2 and in Fig.A2, respectively.

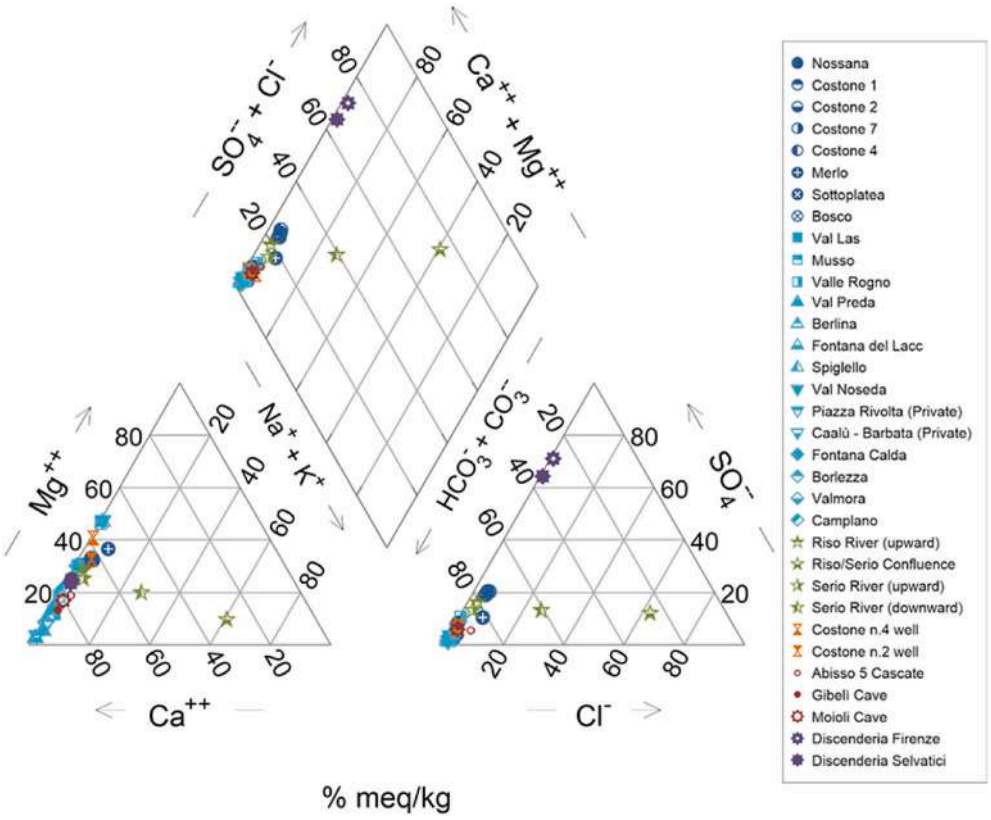

Fig. A1. Piper diagram showing the hydrochemical facies of the sampled waters. All samples have a robust magnesium-bicarbonate signature except the Riso/Serio confluence (sampling point β) (enrichment in Na^+, K^+, and Cl^-, Sodium – Chloride type) and the Mine waters (with high SO_4^{2-}, Calcium chloride type).

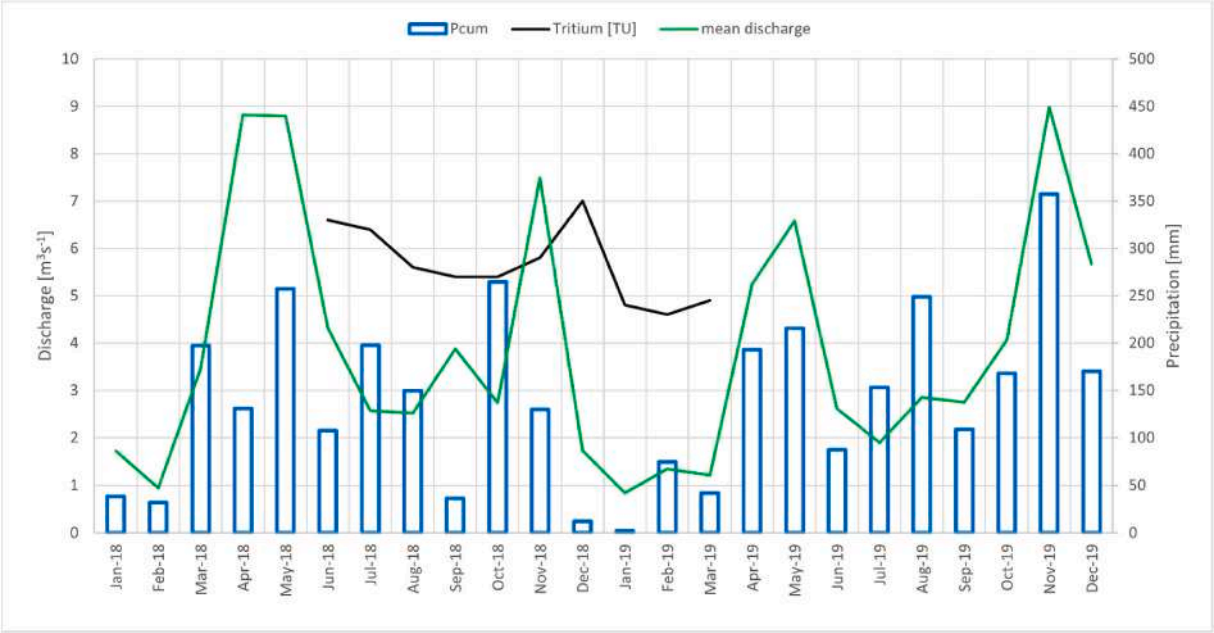

Fig. A2. Variation of tritium content for the Nossana spring waters in relation to the monthly mean discharge and precipitation.

Table A1
Chemical values of water sampled between September 2015 and July 2019.

					Chemical data										
ID	Name	#	Sampling date		Calcium	Magnesium	Potassium	Sodium	Bicarbonate	Chloride	Nitrate	Sulphate	Alkalinity	Ec	pH
Spring water					[mg/l] Ca	[mg/l] Mg	[mg/l] K	[mg/l] Na	[mg/l] HCO_3	[mg/l] Cl	[mg/l] NO_3	[mg/l] SO_4	[mg/l] $CaCO_3$	[µS/cm]	–
A	Nossana	1	September 08, 2015	A1	42.4	8.4	<0.5	1	146	<2	5	13	121	227	8.1
		2	May 21, 2018	A2	34.3	6.9	<0.5	<1	137	<2	3	5	114	186	8.1
		3	June 18, 2018	A3	38	7.4	<0.5	1	138	<2	3	10	115	217	8.1
		4	July 23, 2018	A4	37.9	7.4	<0.5	1	136	<2	4	7	113	215	8
		5	August 27, 2018	A5	36.5	7.9	<0.5	<1	144	<2	4	8	119	209	8
		6	September 24, 2018	A6	38.1	7.8	<0.5	1	137	<2	4	12	114	223	8
		7	October 22, 2018	A7	34.7	7.9	<0.5	<1	140	<2	4	9	116	207	7.8
		8	November 19, 2018	A8	39.2	7.6	<0.5	1	–	<2	3	11	–	219	8
		9	December 17, 2018	A9	38.1	8.1	<0.5	1	129	1	4	12	107	214	8.1
		10	January 29, 2019	A10	36.1	8.3	<0.5	1	134	<2	4	11	111	214	7.9
		11	February 25, 2019	A11	39.5	8.9	<0.5	1	140	<2	4	20	116	242	8
		12	March 25, 2019	A12	35.9	8.4	<0.5	1	137	3	7	12	114	210	8
		13	May 06, 2019	A13	41.1	6.9	<0.5	1	135	<2	5	5	112	201	8
		14	July 22, 2019	A14	37.2	7.8	<0.5	<1	155	<2	4	10.1	128	201	7.9
B	Costone 1	1	May 21, 2018	B1	64.7	18.7	0.8	4	237	7	5	42	195	403	7.6
		2	June 18, 2018	B2	65.9	20.4	1.1	5	236	8	5	51	195	445	7.7
		3	July 23, 2018	B3	62.4	18.2	1.1	4	227	7	5	41	187	407	7.6
		4	August 27, 2018	B4	63.7	20.9	1.3	5	228	8	5	46	188	427	7.7
		5	September 24, 2018	B5	70.4	21.5	1.3	6	228	10	5	55	188	458	7.7
		6	October 22, 2018	B6	66.2	23.3	1.3	6	251	10	5	58	207	459	7.6
		7	November 19, 2018	B7	68.1	16.9	1.1	4	305	8	5	41	252	424	7.7
		8	December 17, 2018	B8	65.6	20.8	1.3	5	222	9	5	50	184	435	7.9
		9	January 29, 2019	B9	65.5	23	1.5	6	224	8	5	46	185	458	7.7
		10	February 25, 2019	B10	62.2	22.2	1.4	6	231	11	5	57	190	445	7.6
		11	March 25, 2019	B11	61.4	22	1.7	7	229	11	5	55	189	447	7.6
		12	May 06, 2019	B12	66.8	15.7	1.1	4	212	6	6	30	175	376	7.7
		13	July 15, 2019	B13	63	20.8	1.99	7.3	–	15.7	5	55.8	–	445	7.6
C	Costone 2	1	September 08, 2015	C1	63.4	21.2	1.6	5	222	10	5	53	183	417	7.7
		2	May 21, 2018	C2	60.7	17.3	1.1	4	225	7	5	39	186	382	7.7
		3	June 18, 2018	C3	62.7	19.3	1.1	5	225	8	5	47	186	416	7.7
		4	July 22, 2019	C4	63.8	20.7	2.18	6.3	305	12.1	4.9	52	251	421	7.6
D	Costone 4	1	May 21, 2018	D1	64	18.4	0.9	4	235	7	5	41	194	402	7.7
		2	June 18, 2018	D2	52.6	17.9	0.7	2	240	8	5	51	198	439	7.7
		3	July 15, 2019	D3	64.2	21.3	1.7	6.7	218	14.8	4.9	56	180	448	7.6
E	Costone 7	1	September 07, 2015	E1	69.5	23.4	1.2	5	245	9	5	58	202	448	7.7
		2	May 21, 2018	E2	64.6	18.8	1	4	245	7	5	41	202	407	7.7
		3	June 18, 2018	E3	66.4	20.6	0.9	5	248	8	5	49	205	440	7.7
		4	July 23, 2018	E4	63.5	18.6	1.1	4	232	7	5	40	191	414	7.6
		5	August 27, 2018	E5	65	21.1	1.3	5	235	9	5	46	194	435	7.6
		6	September 24, 2018	E6	71.2	21.7	1.3	6	229	11	5	57	189	463	7.7
		7	October 22, 2018	E7	65.3	23.1	1.4	6	238	11	5	62	196	461	7.6
		8	November 19, 2018	E8	70.2	17.6	1.1	4	224	8	6	42	185	436	7.7
		9	December 17, 2018	E9	67.1	21.2	1.3	5	221	10	5	51	183	443	7.9
		10	January 29, 2019	E10	65.4	22.9	1.4	6	233	11	5	56	192	460	7.7
		11	February 25, 2019	E11	65.6	22.6	1.4	6	234	11	5	57	193	447	7.6
		12	March 25, 2019	E12	61.3	22.3	1.6	7	230	12	5	61	190	451	7.7
		13	May 06, 2019	E13	65.1	16.2	1.1	4	221	7	7	31	182	386	7.7

(*continued on next page*)

Table A1 (*continued*)

					Chemical data										
ID	Name	#	Sampling date		Calcium	Magnesium	Potassium	Sodium	Bicarbonate	Chloride	Nitrate	Sulphate	Alkalinity	Ec	pH
Spring water					[mg/l] Ca	[mg/l] Mg	[mg/l] K	[mg/l] Na	[mg/l] HCO_3	[mg/l] Cl	[mg/l] NO_3	[mg/l] SO_4	[mg/l] $CaCO_3$	[µS/cm]	–
		14	July 15, 2019	E14	64.2	21.6	1.23	5.2	–	10.5	5.1	54.6	–	437	7.6
F	Merlo	1	May 21, 2018	F1	50.7	20.9	2.8	7	229	13	5	21	189	382	7.7
		2	July 23, 2018	F2	50.3	20.5	2.9	7	221	13	5	22	182	384	7.7
		3	August 27, 2018	F3	50.5	20	3.4	7	215	14	5	23	177	382	7.7
		4	September 24, 2018	F4	52.2	19.9	3.2	7	208	14	5	23	172	387	7.8
		5	October 22, 2018	F5	45.8	15.7	2	3	207	7	4	6	171	314	7.8
		6	November 19, 2018	F6	53	20.7	2.6	6	217	11	5	19	179	394	7.8
		7	December 17, 2018	F7	49.8	20.3	3.1	7	210	13	5	23	174	385	8
		8	January 29, 2019	F8	46.3	19.5	3.2	7	217	13	5	27	179	384	7.7
		9	February 25, 2019	F9	47.9	19.9	3	7	215	14	5	22	177	375	7.7
		10	March 25, 2019	F10	46.3	19.6	3.2	7	211	15	5	25	174	376	7.7
		11	May 06, 2019	F11	52.7	20.9	2.8	6	213	13	5	19	176	376	7.8
		12	July 22, 2019	F12	51.7	19.6	3.28	7.3	215	15.2	5.2	22.2	177	373	7.7
G	Sottoplatea	1	May 21, 2018	G1	50.5	10.4	<0.5	1	206	<2	4	3	170	281	7.8
		2	July 23, 2018	G2	61.2	7.1	<0.5	1	–	<2	3	<3	–	322	7.7
		3	August 27, 2018	G3	50.8	13.5	0.8	1	211	<2	4	3	174	305	7.7
		4	September 24, 2018	G4	51.4	13.9	1.1	2	206	3	4	4	170	314	7.8
		5	October 22, 2018	G5	47.4	19.8	3.2	7	213	14	5	24	176	379	7.7
		6	November 19, 2018	G6	55.7	11.5	0.5	1	205	<2	4	3	169	312	7.7
		7	December 17, 2018	G7	48.5	14.8	0.7	1	198	2	5	4	164	299	8
		8	January 29, 2019	G8	45.1	16	1	2	195	6	5	10	161	302	7.8
		9	February 25, 2019	G9	45.3	14.5	0.9	2	198	3	5	4	164	321	7.9
		10	March 25, 2019	G10	43	14.3	1.2	2	194	4	4	5	160	284	7.7
		11	May 06, 2019	G11	54.8	11.7	<0.5	1	194	2	4	3	160	279	7.8
		12	July 15, 2019	G12	44.1	15	0.9	1.6	192	3.6	4.4	4.3	159	289	7.8
H	Bosco	1	September 07, 2015	H1	49.9	14.5	1.1	2	218	4	4	4	180	299	7.8
		2	May 21, 2018	H2	49.8	10.4	0.6	1	202	<2	4	3	167	281	7.8
		3	July 22, 2019	H3	45.9	14.8	1.75	2.3	199	4.4	4.4	5.3	164	289	7.8
I	Va Las	1	October 08, 2015	I1	32.8	8.4	<0.5	<1	133	<2	5	6	110	191	7.9
		2	May 22, 2018	I2	31.7	8.3	<0.5	<1	131	<2	6	6	109	188	8.1
		3	July 24, 2019	I3	32.5	8.9	<0.5	<1	125	<2	5.8	7.8	104	186	8.1
L	Musso	1	May 22, 2018	L1	36.3	19.8	<0.5	<1	201	<2	7	4	166	276	7.8
		2	July 24, 2019	L2	38.1	19.7	<0.5	<1	201	<2	6.8	4.2	166	268	7.9
M	Spino	1	May 22, 2018	M1	38.5	20.4	<0.5	<1	203	<2	6	10	168	292	7.8
		2	July 24, 2019	M2	40.6	20.2	<0.5	<1	190	<2	6.3	9.7	157	283	7.8
N	Valle Rogno	1	September 07, 2015	N1	67.2	5.7	0.6	2	208	<2	5	20	172	319	7.9
		2	May 22, 2018	N2	66.8	5.2	0.6	2	212	<2	4	17	175	325	7.6
		3	July 24, 2019	N3	66.1	5.4	0.6	2.3	203	<2	4.1	20	167	315	7.6
O	Val Preda	1	May 29, 2018	O1	61.1	1.8	0.5	1	182	<2	2	3	151	277	8
		2	July 30, 2019	O2	76	2.8	1.48	1.2	225	2.3	6.7	8.2	186	358	7.7
P	Berlina	1	May 29, 2018	P1	63.5	7.5	<0.5	1	213	<2	7	3	176	324	7.8
		2	July 30, 2019	P2	78.8	3.5	0.86	<1	235	<2	7.6	4.1	194	362	7.8
Q	Fontana del Lacc	1	May 29, 2018	Q1	78	1.2	<0.5	1	224	<2	5	3	185	345	7.8
		2	July 30, 2019	Q2	68.2	1.1	<0.5	<1	196	<2	5.9	4	162	301	7.8
R	Spiglello	1	May 29, 2018	R1	28.7	15.9	<0.5	<1	149	<2	6	<3	124	228	8.1
		2	July 26, 2019	R2	29.5	15.6	<0.5	<1	147	<2	5.2	<3	122	215	8
S	Val Noseda	1	May 29, 2018	S1	28.2	16.3	<0.5	<1	150	<2	5	<3	125	230	8.1
		2	July 26, 2019	S2	29.8	15.9	<0.5	<1	146	<2	5.6	<3	121	213	7.8
T	Piazza Rivolta (Privata)	1	May 30, 2018	T1	67	1.2	<0.5	1	190	<2	7	4	157	298	7.8
		2	July 25, 2019	T2	67.2	1.5	<0.5	<1	206	<2	6.7	6.8	170	302	7.8

(*continued on next page*)

Table A1 (*continued*)

					Chemical data										
ID	Name	#	Sampling date		Calcium	Magnesium	Potassium	Sodium	Bicarbonate	Chloride	Nitrate	Sulphate	Alkalinity	Ec	pH
Spring water					[mg/l] Ca	[mg/l] Mg	[mg/l] K	[mg/l] Na	[mg/l] HCO_3	[mg/l] Cl	[mg/l] NO_3	[mg/l] SO_4	[mg/l] $CaCO_3$	[μS/cm]	–
U	Sorgente Caalù - Barbata (Privata)	1	May 30, 2018	U1	69	2.6	0.6	1	202	2	5	3	166	320	7.5
		2	July 25, 2019	U2	80.7	4.3	0.63	2	251	5	4.5	5.3	206	385	7.1
V	Fontana Calda	1	October 08, 2015	V1	54.2	3.3	<0.5	1	177	<2	2	<3	147	236	8
		2	June 21, 2018	V2	37.8	5.1	<0.5	<1	140	<2	2	<3	116	192	8.1
		3	July 26, 2019	V3	35.4	4.7	<0.5	<1	141	<2	2	<3	117	181	8.1
Z	Borlezza	1	June 21, 2018	Z1	51.1	2.9	<0.5	1	162	<2	3	<3	135	235	8.2
		2	July 26, 2019	Z2	50.5	2.9	<0.5	<1	161	<2	2.6	<3	133	232	7.9
X	Valmora	1	September 07, 2015	X1	37.4	9.8	<0.5	<1	155	<2	4	3	129	218	8.1
Y	Camplano	1	September 07, 2018	Y1	46.4	7.4	<0.5	<1	172	<2	2	3	142	239	7.9
		2	July 25, 2019	Y2	40.6	6.9	<0.5	<1	141	<2	<2	3.8	117	219	8
α	Torrente Riso - Monte	1	October 08, 2015	α1	62.3	14.2	1.2	4	206	5	7	44	172	379	8.3
		2	May 30, 2018	α2	49.2	12.6	0.7	3	179	5	5	15	150	298	8.3
		3	July 24, 2019	α3	57.1	15.4	0.75	2.9	194	5	6.3	32.9	163	336	8.4
β	Confluence Riso/Serio	1	September 08, 2015	β1	56.5	16.2	69.6	73	174	170	6	54	152	905	8.8
		2	May 30, 2018	β2	51.2	12.5	28	43	174	80	5	32	146	585	8.4
		3	July 24, 2019	β3	114.1	13.7	197.1	232.6	149	497.6	6	103	128	2019	8.7
ɣ	Fiume Serio - Monte	1	September 07, 2015	ɣ1	36.6	8	1.1	2	121	3	4	17	102	207	8.4
		2	May 30, 2018	ɣ2	29	5.7	0.6	1	96	<2	3	7	80	166	8.1
		3	July 24, 2019	ɣ3	22.5	5.6	1.88	3.3	74	3.7	3.1	12.2	62	136	8.4
Δ	Fiume Serio	1	September 07, 2015	Δ1	–	–	–	–	–	–	–	–	–	–	–
		2	October 08, 2015	Δ2	–	–	–	–	–	–	–	–	–	–	–
		3	May 30, 2018	Δ3	29	6	3	5	96	9	3	10	80	199	8.1
		4	July 24, 2019	Δ4	25.6	6.4	13.38	18	79	35.7	9	19.5	66	282	8.3
X	Pozzo Costone n.4	1	June 18, 2018	Pz-A1	53.8	22.7	0.5	1	263	2	4	13	216	380	7
		2	July 22, 2019	Pz-A2	–	–	–	–	–	–	–	–	–	–	–
Y	Pozzo Costone n.2	1	June 18, 2018	Pz-B1	66.2	20.6	0.9	5	222	3	6	13	183	348	7.7
λ	Abisso 5 Cascate	1	July 01, 2018	Gr-A1	68.9	10.1	0.5	4	235	8	7	13	195	380	8
		2	May 19, 2019	Gr-A2	56.3	7.2	<0.5	5	193	11	4	7	162	300	8.4
μ	Grotta del Gibelì	1	July 01, 2018	Gr-B1	58.7	5.5	0.6	2	186	2	6	13	154	299	8
		2	May 19, 2019	Gr-B2	55.4	4.5	0.5	2	179	2	5	9	150	265	8.3
ω	Grotta Moioli	1	July 01, 2018	Gr-C1	47.4	5.9	0.6	2	162	<2	4	10	134	255	7.8
		2	May 19, 2019	Gr-C2	46	4	0.9	1	156	3	4	5	129	228	8
Ψ	Discenderia Firenze	1	July 01, 2018	Min-A1	105.7	20	0.8	4	145	3	2	226	120	618	8
		2	May 19, 2019	Min-A2	136.8	26.2	1.1	3	146	4	2	358	120	795	7.6
Φ	Discenderia Selvatici	1	July 01, 2018	Min-B1	122.7	24.8	1.1	4	155	4	3	276	128	714	7.9
		2	May 19, 2019	Min-B2	79.1	14.1	0.7	2	139	2	3	155	115	464	8

Table A2
The results of the $^3H/^3He$ sampling were conducted in September 2015 and July 2019. He total, Ne total, $^4He_{rad}$, and $^4He_{tri}$ are expressed in ccSTP/kg. Tritium activities are measured by ^3He ingrowth methods. Tritium results are the average of two samples. The "Apparent age" is calculated assuming a piston-flow model.

Sample ID	Spring altitude	Sampling date	^3H	He total	Ne total	$^3He/^4He$	ΔHe	ΔNe	Δ^4He_{rad}	$^3He^{tri}$	Apparent Age	Recharge time	initial tritium
	[m a.s.l.]		[TU]	[ccSTP/kg]	[ccSTP/kg]		[%]	[%]	[ccSTP/kg]	[ccSTP/kg]	[years]		[TU]
A – Nossana	474	Sep-15	5.7 ± 0.2	6.1E-05	2.5E-04	1.5E-06	55.7	43.4	<1E-6	6.2E-12	6.5	2009.3	8.1

(*continued on next page*)

Table A2 (*continued*)

Sample ID	Spring altitude	Sampling date	^{3}H	He total	Ne total	$^{3}He/^{4}He$	ΔHe	ΔNe	$\Delta^{4}He_{rad}$	$^{3}He^{tri}$	Apparent Age	Recharge time	initial tritium
	[m a.s.l.]		[TU]	[ccSTP/kg]	[ccSTP/kg]		[%]	[%]	[ccSTP/kg]	[ccSTP/kg]	[years]		[TU]
			5.7 ± 0.2	6.1E-05	2.5E-04	1.5E-06	54.5	42.5	<1E-6	5.8E-12	6.1	2009.7	8.0
		Jul-19	5.4 ± 0.4	6.2E-05	2.5E-04	1.6E-06	40.9	41.7	9.2E-07	13.7E-12	12.5	2007.1	10.8
			5.4 ± 0.4	6.4E-05	2.6E-04	1.6E-06	44.2	44.6	9.1E-07	14.1E-12	12.8	2006.8	11.0
C – Costone 2	430	Sep-15	5.5 ± 0.2	7.2E-05	2.6E-04	2.0E-06	49.6	39.7	8.3E-06	58.5E-12	29.6	1986.1	29.0
		Jul-19	4.7 ± 0.4	7.3E-05	2.6E-04	2.0E-06	49.6	39.7	9.2E-06	60.6E-12	32.4	1987.3	29.1
N – Valle Rogno	711	Sep-15	4.8 ± 0.2	5.8E-05	2.4E-04	1.5E-06	48.8	37.9	<1E-6	5.5E-12	6.7	2009.1	7.0
		Jul-19	4.8 ± 0.8	5.4E-05	2.3E-04	1.4E-06	38.0	29.5	<1E-6	3.3E-12	4.3	2015.4	6.1
			4.8 ± 0.8	5.7E-05	2.4E-04	1.5E-06	45.8	35.5	<1E-6	4.3E-12	5.4	2014.2	6.5
X – Valmora	1770	Sep-15	5.5 ± 0.2	4.0E-05	1.8E-04	1.4E-06	4.0	3.1	<1E-6	1.4E-12	1.7	2014.1	6.0
Y – Camplano	1840	Sep-15	5.4 ± 0.2	4.0E-05	1.8E-04	1.4E-06	6.3	4.8	<1E-6	0.2E-12	0.2	2015.6	5.5
		Jul-19	5.8 ± 0.4	4.1E-05	1.8E-04	1.4E-06	7.6	5.8	<1E-6	1.5E-12	1.8	2017.9	6.4

References

Andrews, J.N., 1985. The isotopic composition of radiogenic helium and its use to study groundwater movement in confined aquifers. Chem. Geol. 49 (1–3), 339–351. https://doi.org/10.1016/0009-2541(85)90166-4.

Andrews, J.N., 1992. Mechanisms for noble gas dissolution by groundwaters. In: Isotopes of Noble Gases as Tracers in Environmental Studies. IAEA, Vienna, pp. 87–110.

Asante, J., Dotson, S., Hart, E., Kreamer, D.K., 2018. Water circulation in karst systems: comparing physicochemical and environmental isotopic data interpretation. Environ. Earth Sci. 77 (11), 421. https://doi.org/10.1007/s12665-018-7596-y.

Assereto, R., Jadoul, F., Ometto, P., 1977. Stratigrafia e metallogenesi del settore occidentale del distretto a Pb, Zn, fluorite e barite di Gorno (Alpi Bergamasche). Rev. Ital. Paleontol. Stratigr. (83), 395–532.

Barry, R.G., Chorley, R.J., 2009. Atmosphere, Weather and Climate, 0 ed. Routledge. https://doi.org/10.4324/9780203871027.

Beretta, G.P., Galli, A., Pezzera, G., 1989. Influenza della struttura idrogeologica della Pianura bergamasca sull'inquinamento da atrazina delle acque sotterranee, vol. 22. Acque Sotterranee.

Beyerle, U., 1999. *Groundwater Dynamics, Paleoclimate and Noble Gases* [Doctoral Dissertation, Diploma Thesis]. ETH Zurich.

Capellini, P., 1990. Acqua e Acquedotti nella Storia di Bergamo. Ferruccio Arnoldi Editore.

Ceriani, M., Carelli, M., 2000. Carta delle precipitazioni medie, massime e minime annue del territorio alpino della Regione Lombardia (registrate nel periodo 1891 – 1990) [Mappa].

Chemseddine, F., Dalila, B., Fethi, B., 2015. Characterization of the main karst aquifers of the Tezbent Plateau, Tebessa Region, Northeast of Algeria, based on hydrogeochemical and isotopic data. Environ. Earth Sci. 74 (1), 241–250. https://doi.org/10.1007/s12665-015-4480-x.

Citrini, A., Camera, C.A.S., Alborghetti, F., Beretta, G.P., 2021. Karst groundwater vulnerability assessment: application of an integrative index-based approach to main catchments of middle Valseriana springs (Northern Italy). Environ. Earth Sci. 80 (17), 610. https://doi.org/10.1007/s12665-021-09860-8.

Citrini, A., Camera, C., Beretta, G.P., 2020. Nossana spring (northern Italy) under climate change: projections of future discharge rates and water availability. Water 12 (2), 387. https://doi.org/10.3390/w12020387.

Cook, P.G., Böhlke, J.-K., 2000. Determining timescales for groundwater flow and solute transport. In: Cook, P.G., Herczeg (A c Di), A.L. (Eds.), Environmental Tracers in Subsurface Hydrology. Springer US, pp. 1–30. https://doi.org/10.1007/978-1-4615-4557-6_1.

Davis, J.C., 1986. STATISTICS AND DATA ANALYSIS IN GEOLOGY, third ed.

Delbart, C., Barbecot, F., Valdes, D., Tognelli, A., Fourre, E., Purtschert, R., Couchoux, L., Jean-Baptiste, P., 2014. Investigation of young water inflow in karst aquifers using SF 6 –CFC– 3 H/He– 85 Kr– 39 Ar and stable isotope components. Appl. Geochem. 50, 164–176. https://doi.org/10.1016/j.apgeochem.2014.01.011.

Déri-Takács, J., Erőss, A., Kovács, J., 2015. The chemical characterization of the thermal waters in Budapest, Hungary by using multivariate exploratory techniques. Environ. Earth Sci. 74 (12), 7475–7486. https://doi.org/10.1007/s12665-014-3904-3.

Ecogeo S.r.l., 2007. B.A.S. Bergamo: V.I.A. Regionale. Variante in sanatoria della concessione assentita con D.M.N. 4086 del 26/08/1958 ed aumento della portata di derivazione d'acqua ad uso potabile delle "Sorgenti del Ponte del Costone" in Comune di Casnigo (BG).

Ekwurzel, B., Schlosser, P., Smethie, W.M., Plummer, L.N., Busenberg, E., Michel, R.L., Weppernig, R., Stute, M., 1994. Dating of shallow groundwater: comparison of the transient tracers 3H/3He, chlorofluorocarbons, and 85Kr. Water Resour. Res. 30 (6), 1693–1708. https://doi.org/10.1029/94WR00156.

Erőss, A., Mádl-Szőnyi, J., Surbeck, H., Horváth, Á., Goldscheider, N., Csoma, A.É., 2012. Radionuclides as natural tracers for the characterization of fluids in regional discharge areas, Buda Thermal Karst, Hungary. J. Hydrol. 426–427, 124–137. https://doi.org/10.1016/j.jhydrol.2012.01.031.

ERSAF, 2010. Aggiornamento della base informativa dei suoli della Regione Lombardia in. scala 1, 250.000.

Federazione Speleologica Lombarda, 2011. Osservatorio delle Aree Carsiche Lombarde.

Fioretti, C.S., Zanin, G., Ferrario, P., Vighi, M., 1998. Chemical characteristics: the case of herbicides in Italy. In: Swanson, T.M., Vigh, M. (Eds.), Regulating Chemical Accumulation in the Environment: the Integration of Toxicology and Economics in Environmental Policy-Making. Cambridge University Press, pp. 23–49.

Ford, D., Williams, P.W., 2007. Karst Hydrogeology and Geomorphology. John Wiley & Sons.

Freundt, F., Schneider, T., Aeschbach-Hertig, W., 2013. Response of noble gas partial pressures in soil air to oxygen depletion. Chem. Geol. 339, 283–290. https://doi.org/10.1016/j.chemgeo.2012.07.026.

Gardner, P.M., Heilweil, V.M., 2014. A multiple-tracer approach to understanding regional groundwater flow in the Snake Valley area of the eastern Great Basin, USA. Appl. Geochem. 45, 33–49. https://doi.org/10.1016/j.apgeochem.2014.02.010.

Gattinoni, P., Francani, V., 2010. Depletion risk assessment of the Nossana Spring (Bergamo, Italy) based on the stochastic modeling of recharge. Hydrogeol. J. 18 (2), 325–337. https://doi.org/10.1007/s10040-009-0530-3.

GeoTer, 2000. B.A.S. Bergamo: Sorgenti del Costone in Comune di Casnigo. Domanda di Rinnovo di Concessione di Derivazione d'acque ad Uso Potabile delle "Sorgenti Del Costone" Comune Di Casnigo (Provincia Di Bergamo).

Gil-Márquez, J.M., Sültenfuß, J., Andreo, B., Mudarra, M., 2020. Groundwater dating tools (3H, 3He, 4He, CFC-12, SF6) coupled with hydrochemistry to evaluate the hydrogeological functioning of complex evaporite-karst settings. J. Hydrol. 580, 124263 https://doi.org/10.1016/j.jhydrol.2019.124263.

Güler, C., Thyne, G.D., 2004. Hydrologic and geologic factors controlling surface and groundwater chemistry in Indian Wells-Owens Valley area, southeastern California, USA. J. Hydrol. 285 (1–4), 177–198. https://doi.org/10.1016/j.jhydrol.2003.08.019.

Hamad, A., Baali, F., Hadji, R., Zerrouki, H., Besser, H., Mokadem, N., Legrioui, R., Hamed, Y., 2018. Hydrogeochemical characterization of water mineralization in

Tebessa-Kasserine karst system (Tuniso-Algerian Transboundry basin). Euro-Mediterranean Journal for Environmental Integration 3 (1), 7. https://doi.org/10.1007/s41207-017-0045-6.
Hartmann, A., Goldscheider, N., Wagener, T., Lange, J., Weiler, M., 2014. Karst water resources in a changing world: review of hydrological modeling approaches: karst water resources prediction. Rev. Geophys. 52 (3), 218–242. https://doi.org/10.1002/2013RG000443.
Heaton, T.H.E., Vogel, J.C., 1981. "Excess air" in groundwater. J. Hydrol. 50, 201–216. https://doi.org/10.1016/0022-1694(81)90070-6.
Hegerl, G.C., Black, E., Allan, R.P., Ingram, W.J., Polson, D., Trenberth, K.E., Chadwick, R.S., Arkin, P.A., Sarojini, B.B., Becker, A., Dai, A., Durack, P.J., Easterling, D., Fowler, H.J., Kendon, E.J., Huffman, G.J., Liu, C., Marsh, R., New, M., et al., 2015. Challenges in quantifying changes in the global water cycle. Bull. Am. Meteorol. Soc. 96 (7), 1097–1115. https://doi.org/10.1175/BAMS-D-13-00212.1.
Helstrup, T., Jørgensen, N.O., Banoeng-Yakubo, B., 2007. Investigation of hydrochemical characteristics of groundwater from the Cretaceous-Eocene limestone aquifer in southern Ghana and southern Togo using hierarchical cluster analysis. Hydrogeol. J. 15 (5), 977–989. https://doi.org/10.1007/s10040-007-0165-1.
Herzberg, O., Mazor, E., 1979. Hydrological applications of noble gases and temperature measurements in underground water systems: examples from Israel. J. Hydrol. 41 (3–4), 217–231. https://doi.org/10.1016/0022-1694(79)90063-5.
Horrocks, D., 2014. Applications of Liquid Scintillation Counting. Elsevier Science.
Hosseinzadehtalaei, P., Tabari, H., Willems, P., 2020. Climate change impact on short-duration extreme precipitation and intensity–duration–frequency curves over Europe. J. Hydrol. 590, 125249 https://doi.org/10.1016/j.jhydrol.2020.125249.
IPCC, 2014. Climate Change 2014: Synthesis Report. Contribution of Working Groups I, II and III to the Fifth Assessment Report of the Intergovernmental Panel on Climate Change [Core Writing Team. IPCC, Geneva, Switzerland, p. 151.
Jadoul, F., Berra, F., Bini, A., Ferliga, C., Mazzoccola, D., Papani, L., Piccin, A., Rossi, R., Rossi, S., Trombetta, G.L., 2012. Foglio 077 Clusone. Note Illustrative Della Carta Geologica d'Italia Alla Scala 1:50.000. ISPRA, Servizio Geologico d'Italia. https://air.unimi.it/handle/2434/234475#.X-sHC9hKiiM.
Jadoul, F., Pozzi, R., Pestrin, S., 1985. La sorgente Nossana: Inquadramento geologico e idrogeologico (Val seriana, Prealpi bergamasche). Rivista Museo Scienze Naturali Bergamo, pp. 129–140.
James, E.R., Manga, M., Rose, T.P., Hudson, G.B., 2000. The use of temperature and the isotopes of O, H, C, and noble gases to determine the pattern and spatial extent of groundwater flow. J. Hydrol. 237 (1–2), 100–112. https://doi.org/10.1016/S0022-1694(00)00303-6.
Janković, M.M., 2018. Tritium: Advances in Research and Applications. Nova Science Publishers. A c. Di.
Kaown, D., Koh, D.-C., Lee, K.-K., 2009. Effects of groundwater residence time and recharge rate on nitrate contamination deduced from δ18O, δD, 3H/3He and CFCs in a small agricultural area in Chuncheon, Korea. J. Hydrol. 366 (1–4), 101–111. https://doi.org/10.1016/j.jhydrol.2008.12.016.
Kazemi, G.A., Lehr, J.H., Perrochet, P., 2006. Groundwater Age. Wiley-Interscience.
Kollarits, S., Kuschnig, G., Veselic, M., Pavicic, A., Soccorso, C., Aurighi, M., 2006. Decision-support systems for groundwater protection: innovative tools for resource management. Environ. Geol. 49 (6), 840–848. https://doi.org/10.1007/s00254-006-0179-3.
Lauber, U., Ufrecht, W., Goldscheider, N., 2014. Spatially resolved information on karst conduit flow from in-cave dye tracing. Hydrol. Earth Syst. Sci. 18 (2), 435–445. https://doi.org/10.5194/hess-18-435-2014.
Liu, Z., Li, Q., Sun, H., Wang, J., 2007. Seasonal, diurnal and storm-scale hydrochemical variations of typical epikarst springs in subtropical karst areas of SW China: soil CO2 and dilution effects. J. Hydrol. 337 (1–2), 207–223. https://doi.org/10.1016/j.jhydrol.2007.01.034.
Long, D.T., Voice, T.C., Niagolova, N.D., McElmurry, S.P., 2012. Effects of human activities on karst groundwater geochemistry in a rural area in the Balkans. Appl. Geochem. 27 (10), 1920–1931. https://doi.org/10.1016/j.apgeochem.2012.07.003.
Mainoli, G., 1934. Gli Acquedotti della Città di Bergamo. Anonima Bolis.
Mamyrin, B.A., Tolstichin, L.N., Fyfe, W.S., Tolstichin, I.N., 1984. Helium Isotopes in Nature. Elsevier.
Manning, A.H., Ball, L.B., Wanty, R.B., Williams, K.H., 2021. Direct observation of the depth of active groundwater circulation in an alpine watershed. Water Resour. Res. 57 (2), 2020WR028548 https://doi.org/10.1029/2020WR028548.
Manning, A.H., Caine, J.S., 2007. Groundwater noble gas, age, and temperature signatures in an Alpine watershed: valuable tools in conceptual model development: groundwater signatures in an alpine watershed. Water Resour. Res. 43 (4) https://doi.org/10.1029/2006WR005349.
Manning, A.H., Solomon, D.K., 2003. Using noble gases to investigate mountain-front recharge. J. Hydrol. 275 (3–4), 194–207. https://doi.org/10.1016/S0022-1694(03)00043-X.
Marfia, A.M., Krishnamurthy, R.V., Atekwana, E.A., Panton, W.F., 2004. Isotopic and geochemical evolution of ground and surface waters in a karst dominated geological setting: a case study from Belize, Central America. Appl. Geochem. 19 (6), 937–946. https://doi.org/10.1016/j.apgeochem.2003.10.013.
Matiu, M., Crespi, A., Bertoldi, G., Carmagnola, C.M., Marty, C., Morin, S., Schöner, W., Cat Berro, D., Chiogna, G., De Gregorio, L., Kotlarski, S., Majone, B., Resch, G., Terzago, S., Valt, M., Beozzo, W., Cianfarra, P., Gouttevin, I., Marcolini, G., et al., 2021. Observed snow depth trends in the European Alps: 1971 to 2019. Cryosphere 15 (3), 1343–1382. https://doi.org/10.5194/tc-15-1343-2021.
Mehta, N., Dino, G., Passarella, I., Ajmone-Marsan, F., Rossetti, P., De Luca, D., 2020. Assessment of the possible reuse of extractive waste coming from abandoned mine sites: case study in gorno, Italy. Sustainability 12 (6), 2471. https://doi.org/10.3390/su12062471.
Moeck, C., Popp, A.L., Brennwald, M.S., Kipfer, R., Schirmer, M., 2021. Combined method of 3H/3He apparent age and on-site helium analysis to identify groundwater flow processes and transport of perchloroethylene (PCE) in an urban area. J. Contam. Hydrol. 238, 103773 https://doi.org/10.1016/j.jconhyd.2021.103773.
Mondillo, N., Lupone, F., Boni, M., Joachimski, M., Balassone, G., De Angelis, M., Zanin, S., Granitzio, F., 2020. From Alpine-type sulfides to nonsulfides in the Gorno Zn project (Bergamo, Italy). Miner. Deposita 55 (5), 953–970. https://doi.org/10.1007/s00126-019-00912-5.
NOAA, NASA, USAF, 1976. U.S. Standard Atmosphere. NOAA-S/T, pp. 76–1562.
Nolte, H., MacVicar, T.D., Tellkamp, F., Krüger, M., 2018. Instant Clue: A Software Suite for Interactive Data Visualization and Analysis. Sci Rep 8, 12648. https://doi.org/10.1038/s41598-018-31154-6.
Omenetto, P., Vailati, G., 1977. Ricerche geominerarie nel settore centrale del distretto a Pb-Zn, fluorite e barite di Gorno (Lombardia). L'Industria Min (28), 25–44.
Osenbrück, K., 1991. Laborversuche zur Bildung des Luftüberschusses im Grundwasser (Doctoral dissertation, Diploma thesis). Universitat Heidelberg, Heidelberg, Germany.
Ozyurt, N.N., 2008. Residence time distribution in the Kirkgoz karst springs (Antalya-Turkey) as a tool for contamination vulnerability assessment. Environ. Geol. 53 (7), 1571–1583. https://doi.org/10.1007/s00254-007-0811-x.
Pearson, F.J., 1991. Applied isotope hydrogeology: a case study in Northern Switzerland, Studies in environmental science. Elsevier ; Distributors for the U.S. and Canada. Elsevier Science Pub. Co, Amsterdam ; New York : New York, NY, U.S.A.
Piper, A.M., 1944. A graphic procedure in the geochemical interpretation of water-analyses. Trans. Am. Geophys. Union 25 (6), 914. https://doi.org/10.1029/TR025i006p00914.
Pu, J., Cao, M., Zhang, Y., Yuan, D., Zhao, H., 2014. Hydrochemical indications of human impact on karst groundwater in a subtropical karst area, Chongqing, China. Environ. Earth Sci. 72 (5), 1683–1695. https://doi.org/10.1007/s12665-014-3073-4.
Rumpf, S.B., Gravey, M., Brönnimann, O., Luoto, M., Cianfrani, C., Mariethoz, G., Guisan, A., 2022. From white to green: snow cover loss and increased vegetation productivity in the European Alps. Science 376 (6597), 1119–1122. https://doi.org/10.1126/science.abn6697.
Ryan, M., Meiman, J., 1996. An examination of short-term variations in water quality at a karst spring in Kentucky. Ground Water 34 (1), 23–30. https://doi.org/10.1111/j.1745-6584.1996.tb01861.x.
Santoni, S., Garel, E., Gillon, M., Marc, V., Miller, J., Babic, M., Simler, R., Travi, Y., Leblanc, M., Huneau, F., 2021. Assessing the hydrogeological resilience of a groundwater-dependent Mediterranean peatland: impact of global change and role of water management strategies. Sci. Total Environ. 768, 144721 https://doi.org/10.1016/j.scitotenv.2020.144721.
Schlosser, P., Stute, M., Dörr, H., Sonntag, C., Münnich, K.O., 1988. Tritium/3He dating of shallow groundwater. Earth Planet Sci. Lett. 89 (3–4), 353–362. https://doi.org/10.1016/0012-821X(88)90122-7.
Spada, M., Bertuletti, C., 1988. Studi e indagini per la valutazione della potenzialità idrica della zona medio-alta Valle Seriana. Amministrazione Provinciale di Bergamo.
Stevanović, Z., 2019. Karst waters in potable water supply: a global scale overview. Environ. Earth Sci. 78 (23), 662. https://doi.org/10.1007/s12665-019-8670-9.
Stevenazzi, S., Zuffetti, C., Camera, C.A.S., Lucchelli, A., Beretta, G.P., Bersezio, R., Masetti, M., 2023. Hydrogeological characteristics and water availability in the mountainous aquifer systems of Italian Central Alps: a regional scale approach. J. Environ. Manag. 340, 117958 https://doi.org/10.1016/j.jenvman.2023.117958.
Sültenfuß, J., Roether, W., Rhein, M., 2009. The Bremen mass spectrometric facility for the measurement of helium isotopes, neon, and tritium in water. Isot. Environ. Health Stud. 45 (2), 83–95. https://doi.org/10.1080/10256010902871929.
Swan, A.R.H., Sandilands, M., 1995. Introduction to Geological Data Analysis.
Tolstikhin, I.N., Kamenskii, I.L., Mamyrin, B.A., 1969. ISOTOPIC CRITERION FOR DETERMINATION OF NATURAL HELIUM ORIGIN. Geokhimiya (2), 201–205.
Top, Z., Eismont, W.C., Clarke, W.B., 1987. Helium isotope effect and solubility of helium and neon in distilled water and seawater. Deep-Sea Res., Part A 34 (7), 1139–1148. https://doi.org/10.1016/0198-0149(87)90068-9.
Varlam, C., Stefanescu, I., Duliu, O.G., Faurescu, I., Popescu, I., 2009. Applying direct liquid scintillation counting to low level tritium measurement. Appl. Radiat. Isot. 67 (5), 812–816. https://doi.org/10.1016/j.apradiso.2009.01.023.
Vesper, DorothyJ., White, WilliamB., 2004. Storm pulse chemographs of saturation index and carbon dioxide pressure: implications for shifting recharge sources during storm events in the karst aquifer at Fort Campbell, Kentucky/Tennessee, USA. Hydrogeol. J. 12 (2) https://doi.org/10.1007/s10040-003-0299-8.
Vighi, M., Beretta, G.P., Francani, V., Funari, E., Nurizzo, C., Previtali, F., Zanin, G., 1991. Il problema della contaminazione da Atrazina nelle acque sotterraneee: Un approccio multidisciplinare. INGEGNERIA AMBIENTALE 21, 494–507.
Vigna, B., Banzato, C., 2015. The hydrogeology of high-mountain carbonate areas: an example of some Alpine systems in southern Piedmont (Italy). Environ. Earth Sci. 74 (1), 267–280. https://doi.org/10.1007/s12665-015-4308-8.
Visser, A., Fourré, E., Barbecot, F., Aquilina, L., Labasque, T., Vergnaud, V., Esser, B.K., 2014. Intercomparison of tritium and noble gases analyses, 3 H/3 He ages and derived parameters excess air and recharge temperature. Appl. Geochem. 50, 130–141. https://doi.org/10.1016/j.apgeochem.2014.03.005.

Wang, S.-J., Li, R.-L., Sun, C.-X., Zhang, D.-F., Li, F.-Q., Zhou, D.-Q., Xiong, K.-N., Zhou, Z.-F., 2004. How types of carbonate rock assemblages constrain the distribution of karst rocky desertified land in Guizhou Province, PR China: phenomena and mechanisms. Land Degrad. Dev. 15 (2), 123–131. https://doi.org/10.1002/ldr.591.

Weiss, R.F., 1970. Helium isotope effect in solution in water and seawater. Science 168 (3928), 247–248. https://doi.org/10.1126/science.168.3928.247.

Weiss, R.F., 1971. Solubility of helium and neon in water and seawater. J. Chem. Eng. Data 16 (2), 235–241. https://doi.org/10.1021/je60049a019.

Weiss, R.F., Kyser, T.K., 1978. Solubility of Krypton in water and seawater. J. Chem. Eng. Data 69–72.

White, W.B., 2002. Karst hydrology: recent developments and open questions. Eng. Geol. 65 (2–3), 85–105. https://doi.org/10.1016/S0013-7952(01)00116-8.

Yuan, J., Xu, F., Deng, G., Tang, Y., Li, P., 2017. Hydrogeochemistry of shallow groundwater in a karst aquifer system of bijie city, guizhou Province. Water 9 (8), 625. https://doi.org/10.3390/w9080625.

Zhong, C., Wang, H., Yang, Q., 2022. Hydrochemical interpretation of groundwater in Yinchuan basin using self-organizing maps and hierarchical clustering. Chemosphere 309, 136787. https://doi.org/10.1016/j.chemosphere.2022.136787.